

Poly(D,L-lactide-co-glycolide) Surface-Anchored Biotin-Loaded Irinotecan Nanoparticles for Active Targeting of Colon Cancer

Prabhanjan S. Giram, Ramakrishna Nimma, Anuradha Bulbule, Amit Singh Yadav, Mahadeo Gorain, Nalukurthi Naga Venkata Radharani, Gopal C. Kundu, and Baijayantimala Garnaik*



Cite This: *ACS Omega* 2024, 9, 3807–3826



Read Online

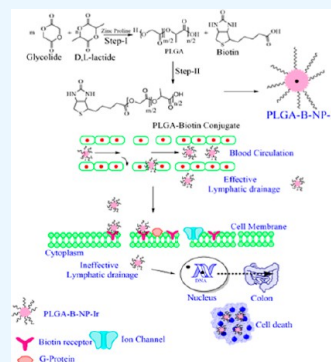
ACCESS |

Metrics & More

Article Recommendations

Supporting Information

ABSTRACT: A poly(D,L-lactide-co-glycolide) (PLGA) copolymer was synthesized using the ring-opening polymerization of D,L-lactide and glycolide monomers in the presence of zinc proline complex in bulk through the green route and was well characterized using attenuated total reflectance–Fourier transform infrared, ¹H and ¹³C nuclear magnetic resonance, gel permeation chromatography, differential scanning calorimetry, X-ray diffraction, matrix-assisted laser desorption/ionization time-of-flight, etc. Furthermore, PLGA-conjugated biotin (PLGA-B) was synthesized using the synthesized PLGA and was employed to fabricate nanoparticles for irinotecan (Ir) delivery. These nanoparticles (PLGA-NP-Ir and PLGA-B-NP-Ir) were tested for physicochemical and biological characteristics. PLGA-B-NP-Ir exhibited a stronger cellular uptake and anticancer activity as compared to PLGA-NP-Ir in CT-26 cancer cells (log *p* < 0.05). The accumulation and retention of fluorescence-labeled nanoparticles were observed to be better in CT-26-inoculated solid tumors in Balb/c mice. The PLGA-B-NP-Ir-treated group inhibited tumor growth significantly more (log *p* < 0.001) than the untreated control, PLGA-NP-Ir, and Ir-treated groups. Furthermore, no body weight loss, hematological, and blood biochemical tests demonstrated the nanocarriers' nontoxic nature. This work presents the use of safe PLGA and the demonstration of a proof-of-concept of biotin surface attached PLGA nanoparticle-mediated active targeted Ir administration to combat colon cancer. To treat colon cancer, PLGA-B-NP-Ir performed better due to specific active tumor targeting and greater cellular uptake due to biotin.



1. INTRODUCTION

The emergence of poly(D,L-lactide-co-glycolide) (PLGA) copolymer in drug delivery application has revolutionized modern drug delivery for chemotherapy. PLGA exhibits tremendous research interest due to its excellent low immunogenicity, biocompatibility, biodegradability, and desired mechanical properties which are very important for the ideal carrier to be used in the drug delivery.^{1,2} The versatility of PLGA controls drug delivery systems by altering the ratio of lactide and glycolide compositions, stereochemistry, catalyst concentration, and molecular weight (\bar{M}_w), which influence polymer properties.^{3–6} Sutures made with synthetic biodegradable polymers, such as Dexon and Vicryl, have been used since 1970.^{7–9} Risperdal, Consta, Vivitrol, Zoladex, Eligard, Suprecur, Enantone, and Profact, among others, are FDA-approved PLGA-based products used in biomedical applications.^{9–11} Encapsulating an anticancer drug in a polymeric matrix in the nano form (polymeric nanomaterials) protects it from enzymatic breakdown and increases its stability.¹²

Stannous octoate is a commercial catalyst (US-FDA approved) used to produce PLGA where the concentration of tin should be less than 20 ppm for biomedical applications. The removal of toxic tin from the polymer matrix by repeated extraction and purification method enhances the production cost based on current good manufacturing practice (cGMP).

The genetic toxicity caused by the presence of tin in the PLGA microsphere has been demonstrated using the comet test in mesenchymal stem cells (MSCs) and human umbilical vein endothelial cells (HUVECs).¹³ The scientific challenge is the innovative synthesis of nontoxic biomaterials. Polymerization of monomers in the presence of suitable metal complexes yields biocompatible polymers.^{14,15}

We synthesized low-molecular-weight D,L-lactide-co-glycolide copolymers (PLGA) with zinc L-proline (Zn-proline) through the green route, tested its biocompatibility using *in vivo* study, and reported them to be nontoxic and safe for biomedical use.¹⁶ Similarly, using the same biocompatible initiator (Zn-proline), we synthesized the poly(ethylene glycol)-*block*-poly(L-lactide-co-glycolide) copolymer in our laboratory and utilized it as a polymer carrier for targeted irinotecan delivery to combat colon cancer *in vivo*.¹⁷ The drug release (paclitaxel–methylene blue conjugate) from poly(lactic-co-glycolic acid) (PLGA) nanoparticles (NPs) (nanocarriers) with redox activity.¹⁸

Received: October 8, 2023

Revised: December 18, 2023

Accepted: December 21, 2023

Published: January 10, 2024



Colon cancer is the third most common cancer and is the second leading cause of cancer-related deaths worldwide. Most colon cancer patients have localized or distant metastases and need adjuvant therapy after surgery. In metastatic cancer, chemotherapy, biological therapies that target the vascular endothelial growth factor (VEGF), and epidermal growth factor receptor (EGFR) pathway, and immunotherapy increase patients' survival.¹⁹

Irinotecan (Ir), is a semisynthetic BCS-II DNA topoisomerase I inhibitor and damages DNA through replication and transcription. Nausea, diarrhea, vomiting, and neutropenia side effects limit its clinical success. The solubility of Ir is 1.07×10^{-1} g/L (pH = 4) and the efficacy is reduced due to low solubility and high permeability. The overexpression of *p*-glycoprotein efflux in cancer cells increases Ir resistance, reduced Ir metabolite formation, and causes toxicity.²⁰ To overcome the formulation barrier of Ir, more effective and targeted delivery strategies are required to increase the local Ir concentration at the targeted site while minimizing side effects to healthy tissues. Cancer treatment practices 1381 out of 1575 nanoformulations registered for clinical trials.^{21–26}

PLGA polymeric NPs are not only biodegradable, biocompatible, and nontoxic, but they also have other benefits such as reduced frequency of administration, lower dose, active targeting, prolonged drug release, and less systemic adverse effects.²⁷ To achieve active tumor-targeting, these polymer NPs can be functionalized with a specific ligand, such as folic acid, saccharides, biotin, peptides, vitamins, antibodies, aptamers, and antibody fragments.^{27,28} The delivery strategy targets the colon which improves to provide specific drugs to the diseased site, increases drug bioavailability, and improves response rates.^{29,30}

Biotin has several benefits, for instance, including limited effect on formulation pharmacokinetics and immunogenicity and helps carboxylase enzymes to produce branched chain amino acids and fatty acids and is also essential for cell growth. Solid tumor cells need biotin due to their high metabolic activity, and many tumor cells overexpress biotin, allowing it for diagnostic purpose. Biotin receptor overexpression occurs in several antagonistic cancer cell lines.³¹ Humans have two biotin transporters: sodium-dependent multivitamin transporter (SMVT) and high-affinity biotin transporter, which are available for biotin uptake in the cell. Human keratinocytes and peripheral blood mononuclear cells have biotin uptake saturation dependent at 10 μ M and 10 nM, respectively. The biotin-targeted nanocarrier system mainly requires SMVT for endocytosis to encourage the selective targeting of NPs and promote the delivery of the hydrophilic drug, which cannot easily cross the cell membrane. Desthiobiotin, lipoic acid, pantothenic acid, and biotin analogues compete with SMVT-mediated biotin uptake, and cancer cells exhibit a higher biotin uptake or SMVT expression.^{32,33}

In the literature, biotin-decorated PLGA developed by DCC/NHS cross coupling and the residual traces of byproduct, dicyclohexylurea (DCU), are difficult to remove and confirm toxicity. This conjugated PLGA has been used to prepare SN-38 encapsulated NPs for active targeting, improve pharmaceutical delivery to cancer cells, and decrease side effects on healthy tissues. However, the toxic metabolite produced from SN-38, caused gastrointestinal damage and diarrhea.³⁴ Biotin-functionalized PEGylated poly(amidoamine) dendrimer conjugation improved paclitaxel solubility and active targeting to lung cancer (A549) cell lines.³⁵ The biotin-decorated lipid nanostructure was developed to overcome the systemic side effects of sunitinib

in lung chemotherapy by active targeting to A549 cell lines.³³ Biotin-conjugated multilayer PLGA–lecithin–polyethylene glycol NPs enabled targeted delivery of doxorubicin, demonstrating considerable in vivo tumor development and an effective delivery for tumor-targeting treatment.³⁶ C₂-streptavidin's receptor-mediated endocytosis of biotin-conjugated tumor suppressor protein P53 into tumor cells proved the usefulness of biotin's targeting ligand.³⁷ Due to the overexpressed biotin receptor, biotin-conjugated gold NPs showed delivery to HeLa cell xenograft mice and decreased tumor growth by 3.8-fold.³⁸

In our previous study, we synthesized the low-molecular-weight D,L-lactide-*co*-glycolide copolymer (PLGA) using zinc L-proline (Zn-proline) in bulk using green synthetic approach and evaluated its biocompatibility in vivo.¹⁶ In continuation of our previous work, we investigate the systematic synthesis of PLGA by the ring opening polymerization of D,L-lactide and glycolide in the presence of Zn-proline complex to generate copolymers ranging from low \bar{M}_w (11,000 Da) to high \bar{M}_w (90,000 Da) and polydispersity (PDI \leq 2). Because of the effective conjugation technique under mild conditions and the nontoxic byproduct, diisopropyl urea, the synthesized PLGA ($\bar{M}_w = 21,000$) was employed as a precursor for conjugation reaction with biotin ligand using diisopropyl carbodiimide. Biotin-conjugated PLGA and PLGA copolymer ($\bar{M}_w = 21,000$) were used as the matrix for NPs formulations for active targeted delivery of Ir. It is apparent that the demonstrated method has the potential for drug delivery (Ir) as a proof of concept to combat cancer, where the drug cannot easily cross cell membranes. The nanoprecipitation technique was used to encapsulate Ir in PLGA (PLGA-NP-Ir) and biotin conjugated copolymer PLGA-B (PLGA-B-NP-Ir), and the physicochemical characterization of these nanoformulations was performed successfully. In the biotin-expressing CT-26 cell line, the cytotoxicity, active targeting, and cellular uptake properties of PLGA NPs (biotin-targeted or non-biotin-targeted) were investigated. The active targeting efficiency and biodistribution of PLGA-B-NP-Ir in CT-26 xenograft tumor bearing Balb/C mice was studied. Biotin-targeted NPs demonstrated exciting results via active targeting and greater accumulation in biotin-overexpressed tumors. Additionally, in an in vivo animal model, these NPs displayed very high hemocompatibility, biocompatibility, and low toxicity. In the case of CT-26 xenograft tumors, Ir-loaded biotin-targeted NPs demonstrated significant antitumor efficacy as compared to nontargeted NPs.

2. EXPERIMENTAL SECTION

2.1. Materials. D,L-Lactide, glycolide from Corbion PURAC (Netherlands), irinotecan (generous gift from Emcure Pune, India), 1,1'-dioctadecyl-3,3,3',3'-tetramethylindotricarbocyanine iodide (DiR), 1,1'-dioctadecyl-3,3,3',3'-tetramethylindocarbocyanine perchlorate⁴⁻ (DiL), 6-diamidino-2-phenylindole (DAPI), and dialysis tubing (MWCO 2000 Da). Snake skin dialysis tubing (MWCO 10,000 Da) was purchased from Thermo Fisher (USA). Cremophor RH 40, methylene chloride, acetone, absolute ethanol, dimethyl sulfoxide (DMSO), and diethyl ether (ultrapure grades) were obtained from Sigma-Aldrich (India). RPMI-1640 media, fetal bovine serum (FBS), penicillin/streptomycin, trypsin/EDTA, and phosphate-buffered saline (PBS) were obtained from Gibco, Invitrogen (India). All of the reagents were used without further purification.

2.2. Synthesis of PLGA Using Ring Opening Polymerization. The polymerization of L-lactide has been reported with

our research group³⁹ and the same procedure was adopted with some modification for PLGA. The polymerization reaction was carried out in bulk in a sealed glass ampule (inner diameter of 2 and 10 cm in height). Glass ampules were passivated using 20% in trimethylsilyl chloride (TMSCl) dissolved in acetone before polymerization and dried properly in the oven. The addition of monomer and initiator was carried out in a MBRAUN UNilab glovebox. Ampules were subjected to 3–4 freeze-pump-thaw cycles in vacuo. Ampules containing monomers such as D,L-lactide, glycolide, and zinc proline initiator were sealed under vacuum. Ampules were then immersed in a Techne SBL-2D fluidized sand bath previously set at the desired temperature. Ampules were cooled and broken at different time intervals. The solid material containing the PLGA copolymer, unreacted D,L-lactide, and glycolide was dissolved in a small amount of dichloromethane and precipitated in excess *n*-hexane to obtain a pure PLGA copolymer. Polymer samples were dried at 40 °C under a vacuum for 48 h. Similarly, PLGA copolymers (PLGA-1 to PLGA-10) were synthesized and characterized.

2.3. Characterization of PLGA Copolymer. The copolymers were characterized by ¹H NMR, ¹³C NMR, matrix assisted laser desorption/ionization time-of-flight mass spectrometry, differential scanning calorimetry (DSC), gel permeation chromatography (GPC), and attenuated total reflectance–Fourier transform infrared (ATR–FTIR). Detailed methods are illustrated in the [Supporting Information](#) (SI).

2.4. Conjugation Reaction of Biotin with PLGA. The biotin-conjugated polymer was prepared by using *N,N'*-diisopropylcarbodiimide (DIPC)/4-dimethylaminopyridine (DMAP) in dry dimethylformamide (DMF) as described in the earlier literature with some modification.³³ Biotin (25 mg, 0.102 mmol) was added to a two-neck round-bottom flask (RBF) 50 mL, and then DIPC (18.2 mg, 0.144 mmol) was added simultaneously with stirring under an inert atmosphere. Finally, the catalytic amount of DMAP was added and the reaction mixture was stirred at 25 °C for 24 h. The obtained functionalized biotin was used for conjugation. The hydroxy-terminated poly(D,L-lactide-*co*-glycolide) (1.296 g, 0.102 mol) in dry dichloromethane (DCM) was added slowly into the reaction mixture and stirred for 24 h at 25 °C. After completion of the reaction, the reaction mixture was diluted with dichloromethane, and the byproduct DIPC–urea was filtered off. The isopropyl urea byproduct derived from DIPC is claimed to be nontoxic and FDA approved.^{40,41} The white solid product was further purified by dissolution in dichloromethane (CH₂Cl₂), and precipitated with excess *n*-hexane. The reaction mixture was filtered, and the white ppt was redissolved in DCM and finally, precipitated in ice cold diethyl ether. The final product was dialyzed against 2000 Da cut off of dialysis membrane in the presence of phosphate buffer solution until the removal of all unreacted biotin (measured by optical density) and finally lyophilized. The equivalent amount of biotin was conjugated with the carboxyl group of PLGA. In the biotin-conjugated PLGA polymer, 0.099 mmol biotin/mg of polymer sample was calculated. The synthesized biotin conjugated PLGA was used for the formulation of the NPs.

2.5. Formulation of the Nanoparticles. The suitable optimization batch of NPs was performed using the method as reported in the literature with some modification.⁴² All nanoformulations were prepared using a similar nanoprecipitation method. The optimization was achieved by varying the concentrations of PLGA and surfactant. In the optimization process, surfactant was varied from 0.04 to 0.02 (% w/v), Ir to

PLGA ratio was selected as 1:5 and 1:10, and is illustrated in [Table S1](#). The particle size, zeta potential, PDI, and drug encapsulation efficiency of different formulations are depicted in [Table S2](#). In the final optimization batch, 10 mg of PLGA or PLGA–biotin conjugate and 1 mg of Ir were dissolved in 2 mL of acetone. The polymeric Ir solution was added dropwise with a syringe to 5 mL of aqueous Cremophor RH 40 solutions (0.02%, w/v) in deionized water with continuous stirring at 1500 rpm. The NPs were stirred for 3 h to remove the residual organic solvent. The final volume of the colloidal suspension was adjusted to 5 mL after the confirmation of complete removal of the organic solvent. The Ir NP with PLGA and PLGA-B matrices was designated as PLGA-NP-Ir and PLGA-B-NP-Ir NP, respectively.

2.6. Characterization of the Formulated NPs. **2.6.1. Determination of Percentage Encapsulation Efficiency.** The encapsulation efficiency (EE %) of Ir-loaded NPs was determined by measuring the concentration of the free drug in the NP suspension. The unencapsulated Ir was separated by centrifugation. The amount of free drug in the filtrate was measured using a UV–vis spectrophotometer (model UV-1601 PC; Shimadzu, Kyoto, Japan) by measuring the absorbance at 360 nm as previously described.^{43,44}

The EE (%) was calculated by

$$\text{EE (\%)} = \frac{([\text{Drug}]_{\text{total}} - [\text{Drug}]_{\text{free}})}{[\text{Drug}]_{\text{total}}} \times 100$$

The percentage of drug loading efficiency (% LE) was calculated using the following equation

$$\text{LE (\%)} = \frac{\text{Amount of Ir encapsulated (mg)}}{\text{weight of all excipients (polymer and surfactant)}} \times 100$$

2.6.2. Size and Zeta Potential Measurements. NPs size, PDI and zeta potential were determined by using Zetasizer (PCS, Nano ZS90 Zetasizer, Malvern Instruments Corp, U. K). Charge on the NPs surface was determined using a Zetasizer 300HSA (Malvern Instruments, Malvern, UK). Disposable polystyrene cells and disposable plain folded capillary zeta cells were used. The NP suspensions were diluted in deionized water, and measurements were performed at 25 °C. Electrophoretic mobility was used to calculate the zeta-potential using the Helmholtz–Smoluchowski equation. Analysis time was kept for 3 min, and hydrodynamic size was presented as the average value of 20 runs, with triplicate measurements within each run.

2.6.3. Transmission Electron Microscopy. Transmission electron microscopy (TEM) imaging of NPs was carried out using an (FEI Technai G2 T20) instrument with an acceleration voltage of 200 keV. The TEM sample was prepared by transferring the NP suspension (4 mg/mL) onto a 200-mesh carbon-coated copper grid. Samples were blotted away after 30 min incubation, and grids were negatively stained for 10 min at room temperature with freshly prepared, 2% (w/v) phosphotungstic acid aqueous solution. The grids were then washed twice with distilled water and air-dried before imaging.

2.6.4. Atomic Force Microscopy. The atomic force microscopy (AFM) measurements were performed on silicon wafer using a Multimode scanning probe microscope equipped with a Nanoscope IV controller from Veeco Instrument Inc., Santa Barbara, CA. All the AFM measurements were carried out under ambient condition using the tapping-mode AFM probes model Tap190Al purchased from Budget Sensors. The radii of

tips used in this study were less than 10 nm, and their height was $\sim 17 \mu\text{m}$. The cantilever used had a resonant frequency of ca. 162 kHz and nominal spring constant of ca. 48 N/m with a 30 nm thick aluminum reflex coating on the back side of the cantilever of the length $225 \mu\text{m}$. For each sample, three locations with a surface area of $1 \times 1 \mu\text{m}^2$ and $500 \times 500 \text{ nm}^2$, each were imaged at a rate of 1 Hz and at a resolution of 512×512 .

2.6.5. Release Profile In Vitro. In vitro release of Ir from PLGA-NP-Ir and PLGA-B-NP-Ir NPs were performed. 20 mg of NPs were suspended in 10 mL of PBS buffer in a dialysis bag (mol. wt. cutoff: 10,000 Da, Sigma-Aldrich) and sealed. The dialysis bag was kept in 100 mL of PBS buffer solution (pH 7.4) and 50% fetal bovine serum in PBS solution (pH 7.4) at 37°C . The release amount was analyzed at 360 nm using UV–visible spectroscopy PerkinElmer calculated using a calibration curve for Ir dissolved in the same media as the dialysate ($R^2 = 0.99995$ over the range between 1 and $50 \mu\text{g/mL}$).^{43,44} A control experiment was set up alongside in which the same amount of Ir was dissolved in dimethyl sulfoxide (DMSO) and dialyzed for comparison. This control was set up to eliminate the nonspecific adsorption of the drug to the dialysis membrane. The same experimental conditions were used for PLGA-B-NP-Ir.

2.6.6. Thermal Characterization by DSC. Thermal analysis was performed with a DSC (DSC Q100, TA Instruments) equipped with a refrigerated cooling system. The glass transition temperature (T_g), crystallization temperature (T_c), melting temperature (T_m), enthalpy of crystallization (ΔH_c), and melting enthalpy (ΔH_m) were calculated from the DSC curves. DSC measurements were carried out by heating the samples (Irinotecan, PLGA-B-polymer, PLGA-NP-Ir, and PLGA-B-NP-Ir) from -90 to 250°C at a rate of $10^\circ\text{C}/\text{min}$, holding for 1 min, and cooling to -90°C at a rate of $100^\circ\text{C}/\text{min}$, holding for 1 min at -90°C , followed by repeating the heating cycle at a rate of $10^\circ\text{C}/\text{min}$ up to 250°C . All measurements were performed under an atmosphere of nitrogen. DSC runs from the second heating cycle are presented.

2.6.7. Powder Wide-Angle X-ray Diffraction of Nanoparticles. The NPs were analyzed using wide-angle X-ray diffraction (WAXD) in the range of $2\theta = 5\text{--}55^\circ$ at room temperature (25°C). The WAXRD patterns of NP sample were analyzed by a Philips 1830 X-ray diffractometer (Philips, Almelo, The Netherlands) using a Cu $K\alpha$ source at a ($\lambda = 1.5406 \text{ \AA}$) to get more insights about the nature of the sample.

2.6.8. Shelf Life Stability of Nanoparticles. NP's suspension was sealed in 10 mL glass vials and stored at 4°C for 28 days. The stability of the NP suspension was tested by visual inspection of the physical properties (color, aggregation, phase separation, and opacity) and also by size and zeta-potential measurements. The measurements were taken in triplicate and presented as an average (mean \pm SD).

2.6.9. In Vitro Antitumor Efficacy Studies. The in vitro antitumor efficacy of the blank PLGA-NP, PLGA-B-NP, PLGA-NP-Ir, and PLGA-B-NP-Ir NPs was examined in CT-26 murine carcinoma cells by the MTT assay. Cells were cultured (2×10^4 cells per well) in a 96-well plate in RPMI media supplemented with 10% FBS, 1% penicillin, and 1% streptomycin in 5% CO_2 atmosphere at 37°C . After 24 h of incubation, different concentrations of irinotecan ($5\text{--}100 \mu\text{g/mL}$ dispersed in media), PLGA, PLGA-B, PLGA-Ir, and PLGA-B-Ir NPs were added into wells. Following 24 h of incubation, wells are washed with PBS, and $200 \mu\text{L}$ of MTT (0.5 mg/mL) was added. Formazan crystals formed after 4 h were dissolved in $200 \mu\text{L}$ of DMSO. Optical absorbance was recorded at 570 nm using a

microplate reader (Epoch2, BoiTek). The results were expressed as the percentage cell survival (mean \pm SE) and calculated by using the following equation

$$\% \text{ Cell survival} = \left(\frac{\text{A 570 nm of treated cells}}{\text{A 570 nm of untreated control cells}} \right) \times 100$$

2.6.10. Fluorescence Labeling of NPs. Fluorescent-labeled DiL and DiR dye-loaded NPs were prepared for in vitro uptake and in vivo tumor targeting and biodistribution studies by an in vivo imaging system (IVIS). DiL, emitting in the red region, and DiR, a fluorophore with near-infrared emission, are hydrophobic fluorescent markers that were incorporated into the organic phase at 0.5% (w/v) (dye/organic phase) for in vitro and in vivo studies, respectively. Formulations were protected from light and covered with aluminum foil and utilized for in vitro (PLGA-NP-DiL and PLGA-B-NP-DiL) and in vivo (PLGA-NP-DiR and PLGA-B-NP-DiR) studies.

2.6.11. Cellular Uptake. CT-26 cells were seeded on coverslips at a density of 1×10^5 cells/well. To check the uptake efficiency of the NPs, cells were treated with DiL tagged PLGA and PLGA-biotin NPs (PLGA-NP-DiL and PLGA-B-NP-DiL). After 4 h, media containing NPs were removed, and cells were fixed with 4% paraformaldehyde for 20 min. The coverslips were mounted on top of slides and uptake was visualized using a Leica sp5 confocal microscope. In separate experiments, cells were treated with cold temp (4°C), sodium azide (0.1%), and sucrose (0.5 M) for 1 h as inhibitor of uptake pathways prior to treatment with NPs followed by confocal analysis.

2.6.12. Cell Cycle Analysis. Effect of irinotecan-loaded PLGA-NP-Ir and PLGA-B-NP-Ir on cell cycle progression in CT-26 cells was analyzed by fluorescence-activated cell sorting (FACS). Briefly, CT-26 cells were seeded in a 60 mm dish at a density of 2×10^5 cells/dish and treated with NPs ($50 \mu\text{g/mL}$) for 24 h. After treatment, cells were fixed overnight in 95% ethanol at 4°C and were washed in chilled PBS two times, and the pellet was resuspended in $50 \mu\text{L}$ of RNase A (0.5 mg/mL) and incubated for 20 min at 37°C . After that, $450 \mu\text{L}$ of propidium iodide ($50 \mu\text{g/mL}$) was added. The proportion of cells at different phases of the cell cycle was monitored by an FACS Caliber (BD Biosciences).

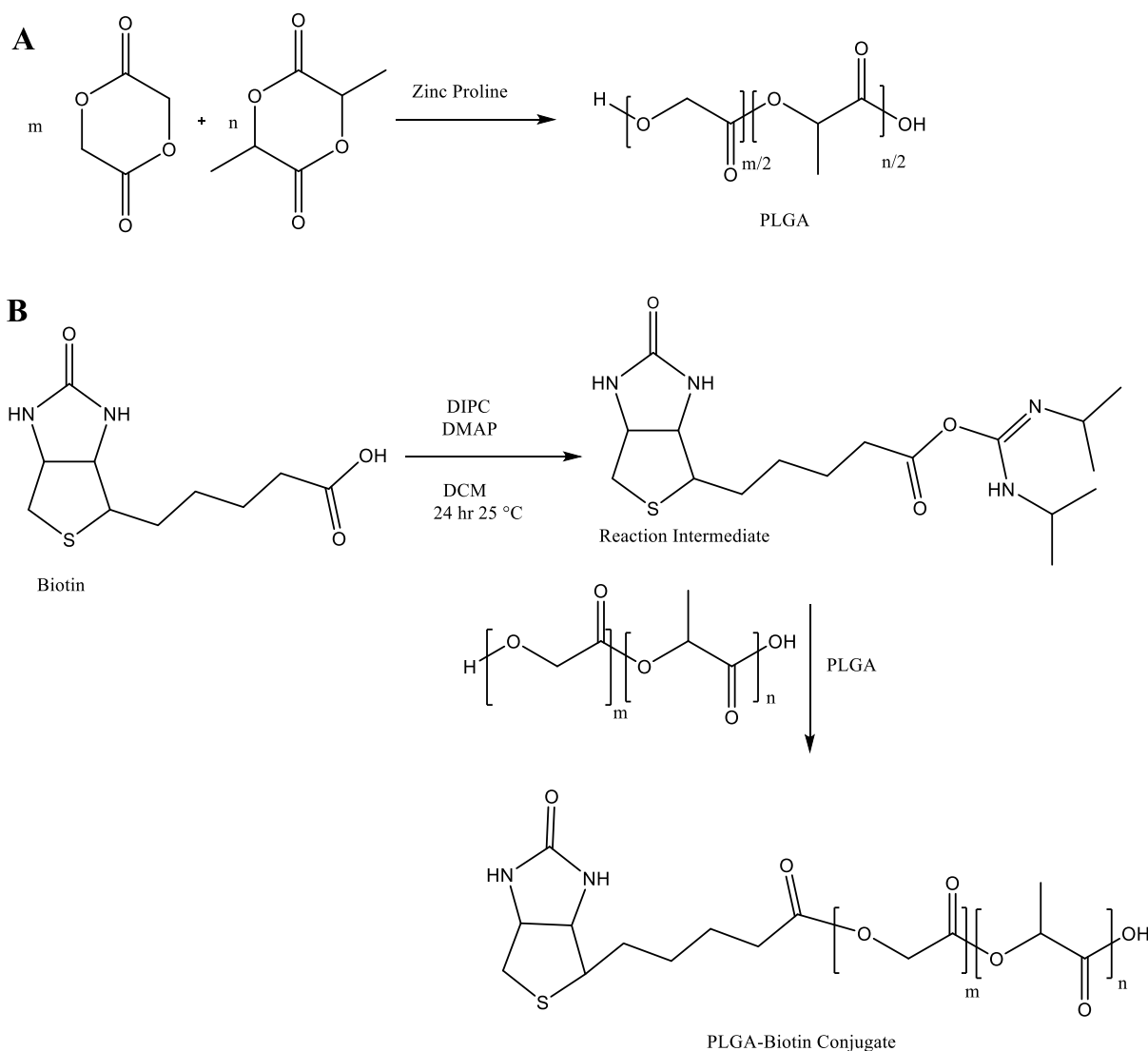
2.6.13. In Vivo Biodistribution Study. All animal procedures were performed in accordance with the guidelines approved by the "Committee for the Purpose of Control and Supervision of Experiments on Animals" (CPCSEA), Government of India. The project entitled "Evaluation of the Anticancer Activity and Pharmacokinetics of Irinotecan NPs in CT-26 cell induced tumor" was approved (EAF animal Ethical approval no: B-286). All experiments were approved by Institutional Animal Care and Use Committee (IACUC) of National Centre for Cell Science (NCCS), Pune, India. 6–8 week's old female BALB/c mice were used to perform the in vivo studies. CT-26 colon cancer cells (1×10^6) mixed with matrigel was injected subcutaneously into the right flanke of mouse, and tumor growth was observed. After tumor generation, DiR-loaded PLGA and PLGA-B loaded NPs (PLGA-NP-DiR and PLGA-B-NP-DiR) were injected intravenously through the tail vein of the mice. The biodistribution of DiR loaded NPs monitored at various time points up to 7 days by in vivo imaging. The biodistribution of the DiR loaded NPs in major organs (heart, lung, liver, spleen, intestine, and kidney) and tumor was examined after 7 days by ex vivo imaging after sacrifice of mice using the IVIS system (IVIS

Table 1. Ring Opening Polymerization of D,L-Lactide and Glycolide

polymer	monomer feed ratio L/G (mol) ^a	monomer incorporation ^b L/G (mol)	temp. (°C)	time (h)	[M ₀]/[I ₀]	\bar{M}_n^c (g/mol)	\bar{M}_w^c (g/mol)	PDI ^c (Đ)
PLGA-1	50:50	48:52	180	3	100	5500	11,000	1.98
PLGA-2	50:50	46:54	180	8	100	5300	12,400	2.34
PLGA-3	50:50	49:51	200	1	200	12,700	21,000	1.65
PLGA-4	50:50	45:55	200	2	200	10,000	18,500	1.85
PLGA-5	50:50	48:52	200	3	200	5600	16,400	2.92
PLGA-6	50:50	46:54	200	4	200	8100	13,900	1.71
PLGA-7	50:50	48:52	200	6	200	8890	16,500	1.85
PLGA-8	50:50	41:59	140	48	1179	29,800	49,700	1.66
PLGA-9	50:50	47:53	140	48	1571	39,870	60,800	1.53
PLGA-10	50:50	49:51	140	48	2361	40,200	87,636	2.18

^aL = lactide, G = glycolide. ^bDetermined by using ¹H NMR spectrum. ^cDetermined using GPC where polystyrene is used as reference, chloroform as eluent.

Scheme 1. Synthesis of the PLGA Copolymer Using Zinc Proline Initiator (A), and Bioconjugation of Biotin to PLGA by the Coupling Reaction (B)



spectrum, Xenogen). In separate experiments, CT-26 tumor bearing mice were injected with (PLGA-NP-DiI and PLGA-B-NP-DiI) and tumor retention of NPs was analyzed for 9 days using IVIS.

2.6.14. In Vivo Tumor Imaging. In vivo fluorescence imaging of PLGA-NP-DiR and PLGA-B-NP-DiR NPs was performed to identify tumor targeting ability and biodistribution of the NPs in living mice bearing CT-26 biotin-enriched colon tumor xenograft models. After systemic administration of DiR loaded

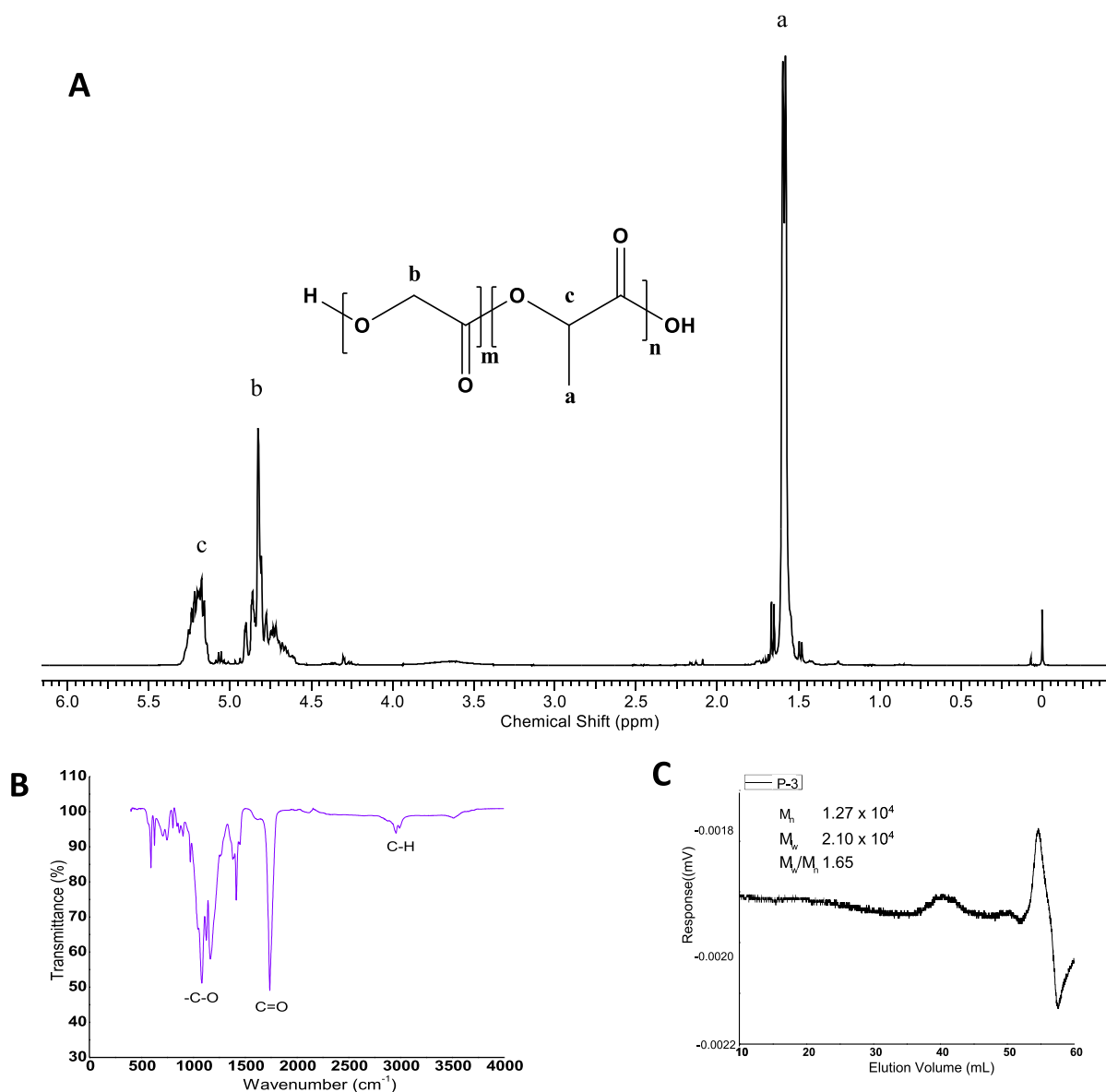


Figure 1. ^1H NMR spectrum (400 MHz) of PLGA-3 in CDCl_3 (A), ATR-FTIR spectrum of PLGA-3 (B), and size exclusion chromatography of PLGA-3 (P-3) (C).

NPs via the tail vein, whole body imaging was monitored up to 72 h. The high intensity fluorescence was detected in the tumor region in both PLGA-NP-DiR and PLGA-B-NP-DiR NPs treated mice which increases over time and reached the maximum at 72 h.

2.6.15. In Vivo Antitumor Efficacy Studies. CT-26 colon cancer cells (1×10^6) mixed with metrogel, was injected subcutaneously into the right flank of female BALB/c mice, and tumor growth was observed. After tumor initiation, mice were treated with irinotecan, PLGA-NP-Ir and PLGA-B-NP-Ir NPs (10 mg/kg body weight corresponding Ir concentration), intratumoral twice a week for 2 weeks. The tumor size was monitored with the help of a Vernier caliper during the experiment. After 2 weeks, mice were sacrificed, and tumors were harvested and weighed. Furthermore, tumor sections were prepared for histopathological analysis.

2.6.16. In Vivo Toxicity Studies. All the experiments illustrated in the project were approved by Institutional Animal Care and Use Committee (IACUC) of National Centre for Cell

Science (NCCS), Pune, India. 6–8 week-old healthy female BALB/c mice were treated with irinotecan, PLGA-NP-Ir, and PLGA-B-Ir NPs (20 mg/kg body weight corresponding to Ir concentration) every day for 1 week. After 1 week, blood was drawn from mice through the retro-orbital sinus and hematological and biochemical analysis was performed to examine the toxicity.

2.6.17. Statistical Analysis. For all experiments, data were presented as mean \pm SD. Significant differences were examined using one-way ANOVA. $p < 0.05$ was considered statistically significant in all studies varied at the highest (M/I) ratio (2361), lowest reaction temperature (140°C), and maximum polymerization time, produced the PLGA copolymer ($\bar{M}_w = 90,000$). Using the ROP of D,L-lactide and glycolide, PLGA ($\bar{M}_w = 21,000$) was prepared using the conditions as shown in Table 1. PLGA of $\bar{M}_w = 21,000$ with PDI = 1.65 was selected and used for bioconjugation with biotin and further nanoformulation of applications because it shows the combination of low molecular weight with comparable narrow PDI, ease of solubility in

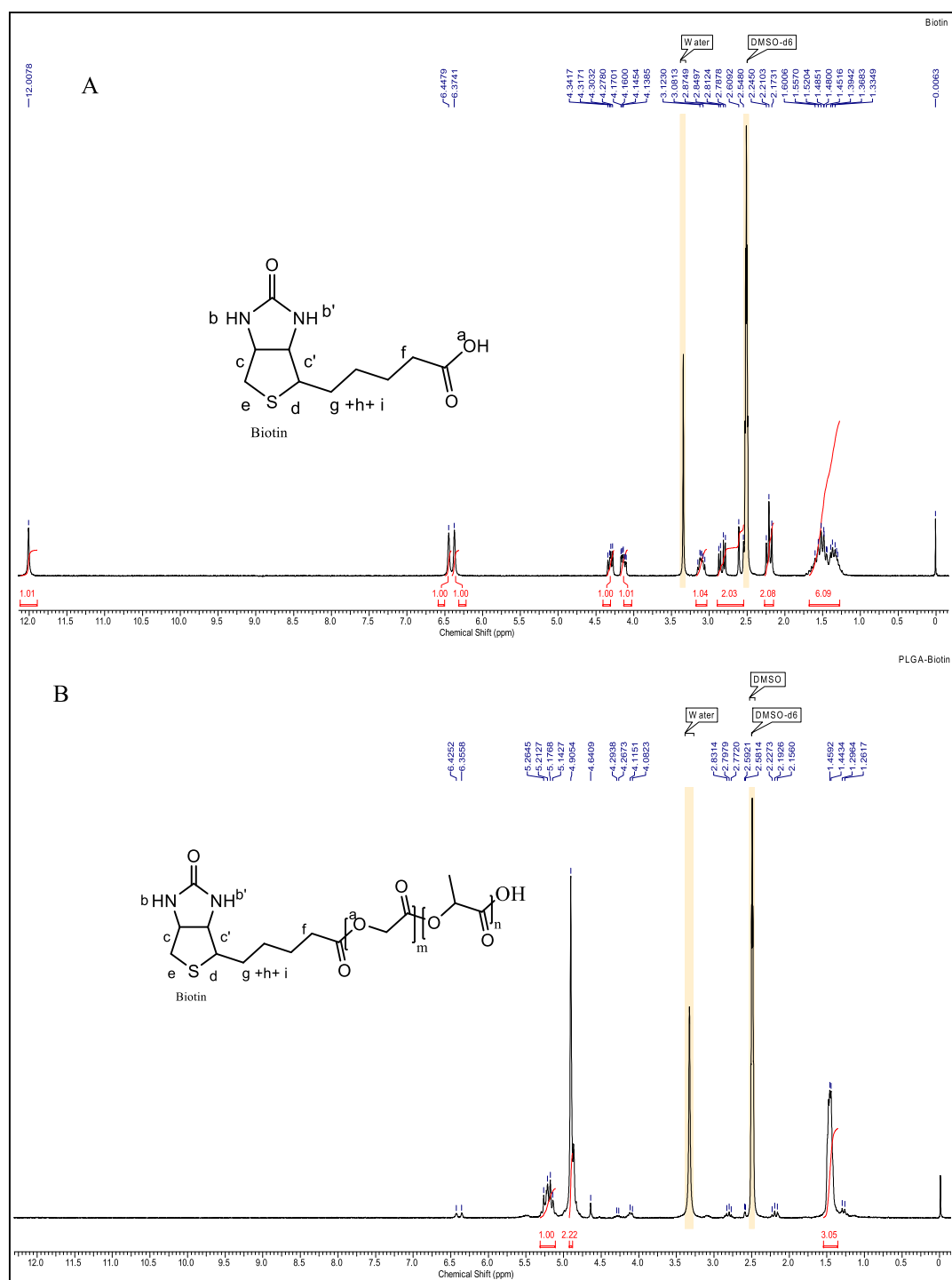


Figure 2. ^1H NMR spectra of biotin (A) and biotin-conjugated PLGA (B).

chloroform, dichloromethane, amorphous in nature, and suitable for drug delivery applications.

3. RESULTS AND DISCUSSION

3.1. Ring Opening Polymerization for PLGA Copolymer. Poly(D,L-lactide-co-glycolide) is a unique copolymer among all synthetic polymers explored worldwide for biomedical applications and has gained huge interest due to its extraordinary biodegradability and biocompatibility properties. Sustained release of PLGA formulations has been clinically approved by the FDA for injectable preparations since 1989.

The most important drug formulated products available in the US market are used for cancer disease, hormonal replacement therapy, dental disorders, and opioid dependence and also provide numerous benefits such as improved patient compliance, reduced dosing frequency, lower drug toxicities, and improved therapeutic actions. PLGA has been prepared commercially by ring opening polymerization using stannous octoate as a catalyst. The removal of toxic tin from the polymer matrix is a scientific challenge that requires extensive purification and extraction steps, at a high cost. With zinc complex initiators, the toxicity concern of tin-based PLGA formulations has been

considerably reduced.^{45–49} Dichloromethane (DCM), has been approved for use in pharmaceuticals as a solvent, typically makes PLGA copolymers soluble.

In this work, we used a zinc proline initiator for the ring opening polymerization of D,L-lactide and glycolide in order to overcome these limitations. The polymerization reaction condition was optimized by varying reaction parameters such as monomer to initiator (*M/I*) ratio, polymerization temperature, and polymerization time at a constant molar monomer feed ratio of D,L-lactide and glycolide (50:50), as shown in Table 1. The polymerization times in Scheme 1A,B show the synthesis of the PLGA copolymer by ring opening polymerization using a zinc proline initiator and bioconjugation of biotin to PLGA by DIPC and DMAP using the coupling reaction, respectively.

The synthesized PLGA exhibited desired molecular weight, molecular weight distribution, and most importantly amorphous in nature. In the literature, the toxic nature of PLGA carrier prepared using stannous octoate suggests a genotoxic effect on cells. A detailed study of the PLGA genotoxic profile in biological systems has been explored to overcome these toxicity issues.¹³ Biotin-conjugated PLGA has been used as a targeting ligand for the tumor because biotin overexpressed its receptor in aggressive tumors like CT-26, breast cancer, pancreatic, and ovarian cancer.^{31,32}

3.2. Characterization of PLGA and PLGA-Conjugated Biotin.

3.2.1. ¹H NMR Spectroscopic Analysis. The structure of the PLGA copolymer was confirmed by the ¹H NMR spectrum, as shown in Figure 1A. The molar compositions of D,L-lactide and glycolide were calculated using ¹H NMR analysis. The CH and CH₃ of lactide appear at 1.52 and at 5.2 ppm and CH₂ of glycolide appears at 4.8 ppm. ¹H NMR has been used for calculation of incorporation ratio for lactide and glycolide and is illustrated in detail. Similar ¹H NMR results have been obtained in the literature.⁵⁰

3.2.2. ¹³C NMR Spectroscopic Analysis. ¹³C NMR analysis of PLGA-3 is depicted in Figure S1 where the carbonyl of lactide and glycolide of PLGA appear at 169 and 165 ppm respectively.

3.2.3. ATR-FTIR Analysis. ATR-FTIR spectrum of the PLGA-3 copolymer is illustrated in Figure 1B. The FTIR spectrum of PLGA exhibited major bands at 1065 cm⁻¹ (O–CH₂ stretching) and 1740 cm⁻¹ (ester C=O stretching). The band appears at 3500 cm⁻¹ (O–H stretching) owing to the terminal hydroxyl groups in the copolymer. The absorptions in the range 2900–3000 cm⁻¹ represent C–H stretching of –CH– and CH₂ band, respectively. These assigned bands confirmed the structure of PLGA and all bands matched to the results reported in the literature.¹⁶

3.2.4. Molecular Weights by Size Exclusion Chromatography. The various molecular weights of synthesized PLGA copolymers were obtained with GPC and are shown in Table 1, and Figure 1C represents the GPC trace where ($\bar{M}_n = 12,700$, $\bar{M}_w = 21,000$, and PDI = 1.65).

The literature studies inspired us to design and synthesize a biocompatible zinc proline initiator to prepare the PLGA copolymer using the ROP technique in bulk through a green route. Subsequently, the PLGA copolymer of ($\bar{M}_w = 21,000$) was synthesized using ROP using D,L-lactide and glycolide in the presence of zinc proline initiator and used for bioconjugation reaction with biotin. Biotin-conjugated PLGA copolymer was used as a drug carrier for irinotecan. Figures S2–S11 show size exclusion chromatography of synthesized PLGA copolymers (PLGA-1 to PLGA-10).

3.2.5. MALDI-TOF Analysis. MALDI-TOF analysis results are shown in Figure S12. The end group of PLGA was analyzed with MALDI-TOF using a DHB (2,5-dihydroxybenzoic acid) matrix. The MALDI-TOF spectra were in the range of 1300–1550. These peaks showed that the D,L-lactide and glycolide were sequentially arranged, and the end groups of PLGA appeared as hydroxyl (–OH) and carboxyl group (–COOH).

$$(LA)_m + (GA)_n + 18 \text{ (OH group of COOH, H)Na}^+, 1340$$

$$(LA)_{m+1} + (GA)_{n+1} + \text{(OH group of COOH, H)}, 1470$$

$$(LA)_{m+2} + (GA)_{n+2} + \text{(OH group of COOH, H)}, 1600$$

$$(LA)_m + (GA)_n + 18 \text{ (OH group of COOH, H)K}^+, 1356$$

$$(LA)_{m+1} + (GA)_{n+1} + 18 \text{ (OH group of COOH, H)K}^+, 1486$$

$$(LA)_{m+2} + (GA)_{n+2} + 18 \text{ (OH group of COOH, H)K}^+, 1616$$

3.2.6. Conjugation of Biotin to PLGA. The biotin-conjugated PLGA was synthesized by the conjugation of biotin with PLGA copolymer, as shown in Scheme 1B. The structure of biotin-conjugated PLGA was confirmed by ¹H NMR as well as fluorescence spectroscopy using the HABA/avidin complex through biotin binding integrity. ¹H NMR of biotin group was known through two methine protons (c, c') from the cyclic biotin structure at 4.2 and 4.3 ppm and two urea protons (b', b) from the cyclic biotin structure at 6.35 and 6.45 ppm. ¹H NMR spectrum of biotin–PLGA conjugate shows; H-d = 3.36, H-c = 4.2, H-c' = 4.3, H-eA = 3.01, H-eB = 2.78, H-f = 2.22, H-i = 2.19, H-h = 2.15, NH-b' = 6.35, NH-b = 6.45, PLA(CH₃) = 1.45, PLA(CH) = 5.16, and PGA (CH₂ = 4.70). The carboxyl group of biotins appeared at 12.0 ppm, as shown in Figure 2A. The NMR spectrum of PLGA–biotin ($\bar{M}_w = 21,000$), the disappearance of the –COOH group at 12.0 ppm occurred, the biotin protons (c, c', b', b) at 4.3, 4.2, 6.33, and 6.45 ppm appeared. However, the peaks at 1.46 (a) and 5.16 (c) ppm regions which are attributed to PLA signals and 4.7 ppm (b) due to the PGA signal, as shown in Figure 2B. In the literature, biotin conjugation has been reported for chitosan as the carrier for cancer drug delivery,⁵¹ biotin-conjugated PLGA by click chemistry has also been reported for doxorubicin hydrochloride delivery to breast cancer sites.⁵² This study reports only an in vitro study. However, no in vivo study has been reported in the details. Avidine shows strong biological noncovalent interaction where four biotin molecules bind to one molecule of avidine due to the availability of four binding sites and the strong association constant of biotin–avidine as compared to avidine–HABA. When biotinylated-PLGA was added to the avidine–HABA sample, the decrease in the absorbance of avidine–HABA was observed due to displacement of the HABA by biotinylated-PLGA schematic presentation, as shown in Figure S13.

The amount of biotin was determined by the following equations

$$\begin{aligned} \Delta A_{500} &= 0.9 \times (\text{HABA/Avidin absorbance}) \\ &\quad - (\text{HABA/Avidin and PEG - biotin} \\ &\quad \text{absorbance}) \end{aligned}$$

$$\text{Biotin concentration (}\mu\text{M)} = (\Delta A_{500}/34) \times 10$$

In the bioconjugation, 0.099 mmol of biotin/mg of polymer sample was calculated.

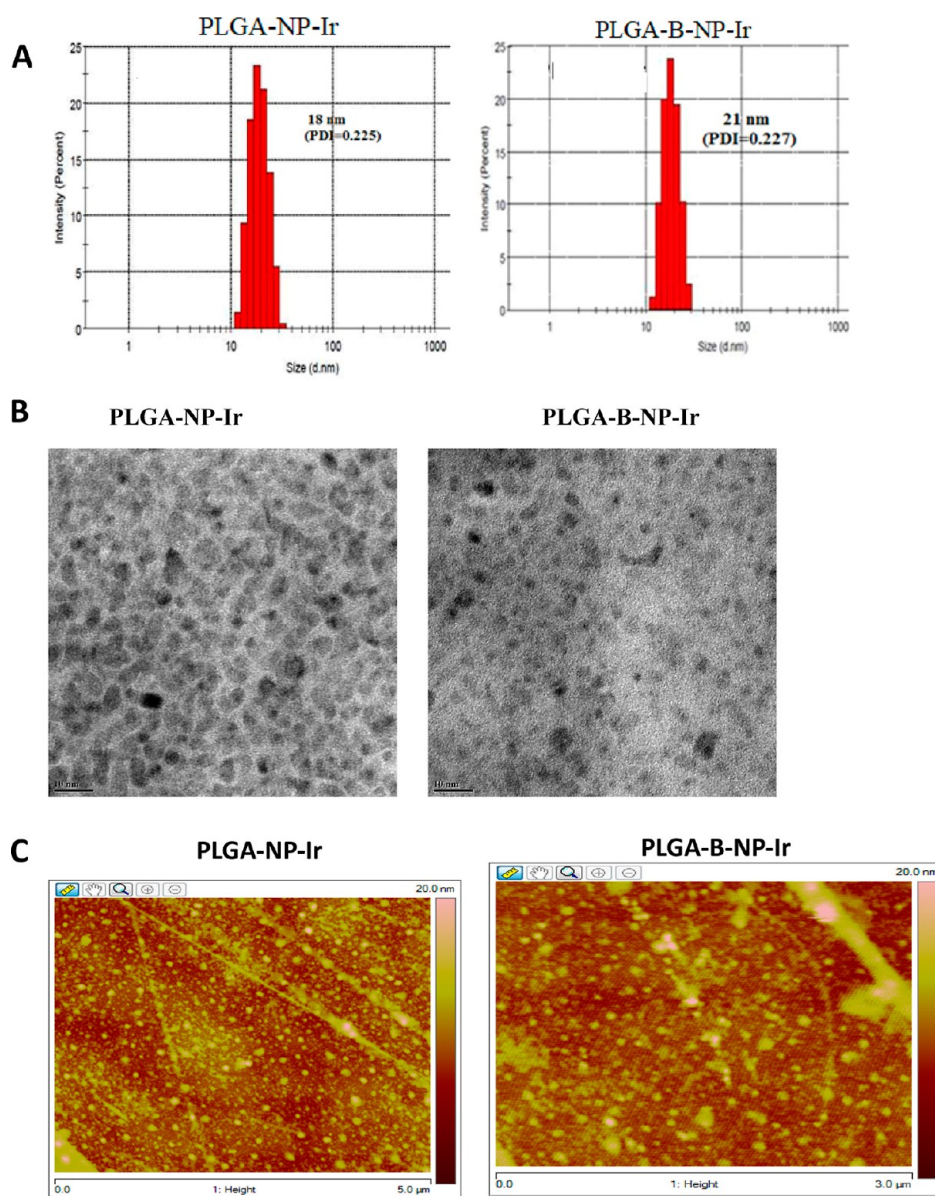


Figure 3. Characterization of NPs: dynamic light scattering particle size distribution (A), TEM analysis (B), and AFM analysis (C).

Table 2. Physicochemical Characterization of PLGA-Based NPs^c

formulation ^a	day	hydrodynamic diameter (nm) ^{b,f}	polydispersity index ^{b,f}	zeta-potential (mV) ^{b,f}	encapsulation efficiency (EE) (%) ^{d,f}	loading efficiency (LE) (%) ^{e,f}
PLGA-Ir	0	18 ± 2.6	0.225 ± 0.04	-15.71 ± 3.9	88.1 ± 3.2	9.5 ± 4.3
	7	21 ± 4.5	0.227 ± 0.03	-14.76 ± 5.4		
	28	25 ± 3.3	0.229 ± 0.02	-13.42 ± 3.4		
PLGA-B-Ir	0	21 ± 5.2	0.227 ± 0.03	-11.15 ± 3.9	80.6 ± 3.5	9.3 ± 5.2
	7	25 ± 7.8	0.228 ± 0.01	-10.13 ± 7.2		
	28	28 ± 2.1	0.229 ± 0.04	-9.4 ± 3.1		

^aIr 5 mg, 25 mg PLGA/PLGA-B, 2 mL acetone, 5 mL distilled water, Cremophor RH 40, 50 mg. ^bMeasured by dynamic light scattering. ^cSurface charge measured by electrophoresis. ^dCalculated as percentage of initial drug added, determined by spectrophotometry. ^eCalculated as mass of incorporated drug divided by the weight of polymer, determined by spectrophotometry. ^fExpressed as mean ± SD ($n = 3$).

The structure of biotinylated-PLGA was confirmed by ¹H NMR and colorimetric analysis.

The biotin-conjugated PLGA was confirmed with ¹H NMR and HABA–avidin colorimetric assay. Similar characterization results have been reported.³³

4. FORMULATION AND PHYSICOCHEMICAL AND MORPHOLOGICAL CHARACTERIZATION OF NPS

The cancer chemotherapy mostly embraces obstacles like low tumor uptake of chemotherapeutic drugs. The poor physicochemical properties of drugs, for instance, poor permeability, solubility, and rapid degradation, to poor bioavailability at the

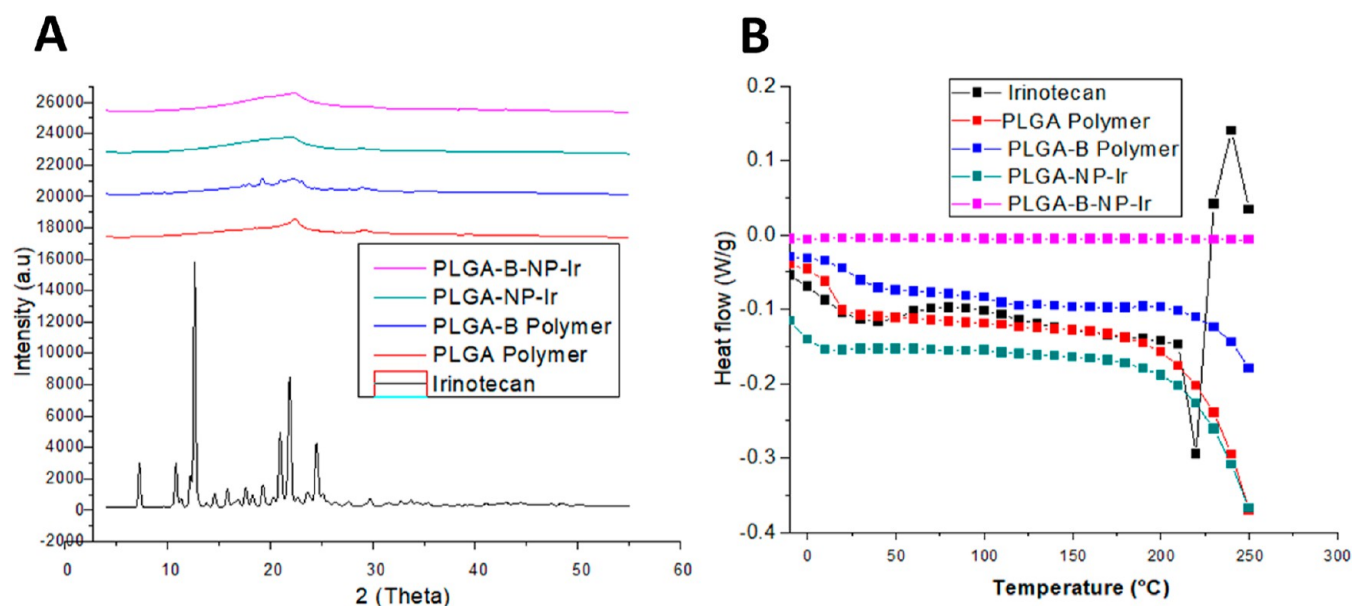


Figure 4. XRD curves of Ir, PLGA, PLGA-B, Ir-loaded PLGA-NP-Ir, and PLGA-B-NP-Ir (A), and DSC curves of Ir, PLGA-B, and Ir-loaded PLGA-NP-Ir and PLGA-B-NP-Ir (B).

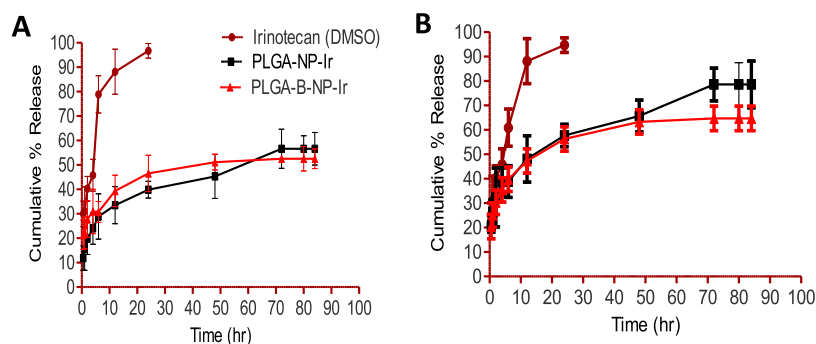


Figure 5. In vitro release study of NPs: PBS, pH 7.4 (A), and 50% serum in PBS, pH 7.4 (B).

tumor region. Irinotecan is sparingly soluble in water and shows many side effects.⁵³ Numerous scientific approaches have been adapted to enhance the water solubility of irinotecan, in addition to better pharmacokinetics. The literature study reveals that several applications of PLGA NPs and nanofibers have been made in several cancer diseases such as glioma, breast, and pancreatic cancer and also target cancer stem cells. However, there are a few literature reports available so far where irinotecan formulation has been used in chemotherapy against colorectal cancer.^{54–56} The nonionic solubilizer and emulsifying agent (Cremophor RH 40) is generally used herewith to solubilize hydrophobic active drug (irinotecan) in purely aqueous solutions. NP formulation was carried out using the nanoprecipitation method using Cremophor RH 40 as a surfactant.⁴² NP was well characterized for physicochemical, morphological, thermal properties, stability, and shelf life study.

NPs were formulated using synthesized PLGA and biotin-decorated PLGA as matrices. The nanoformulation was prepared by nanoprecipitation method and designated Ir-loaded PLGA (PLGA-NP-Ir) and Ir-loaded PLGA-B (PLGA-B-NP-Ir). All nanoformulations were prepared using a similar nanoprecipitation method. In the optimization process, the surfactant was varied from 0.04 to 0.02 (% w/v), Ir to PLGA ratio was selected as 1:5 and 1:10, and is illustrated in Table S1. The particle size, zeta potential, PDI, and drug encapsulation

efficiency of different formulations are depicted in Table S2. Zeta potential is generally related to the charge on the surface of the NP and so influences a wide range of properties of colloidal materials, such as their stability, interaction with electrolytes, and suspension rheology.

The P-3 batch of NPs with surfactant 0.02 (w/v) and drug to polymer ratio (1:5) exhibited particle size of 18 nm and zeta potential of -15 mV which was used as optimized batch for further characterization because of the least particle, as shown in Figure 3A. There was no significant difference in average size between PLGA-NP-Ir and PLGA-B-NP-Ir formulations as shown in Figure 3A, which was measured by dynamic light scattering. The homogeneity of all the formulations was confirmed by PDI which was lower than 0.3.

The negative zeta-potential was observed in the range of -10 to -15 mV which was imparted by the PLGA polymer to NPs and displayed similar physicochemical characteristics. Table 2 shows the encapsulation efficiency (EE %) of the drug in NPs, ranging from 80 to 88%. The encapsulation of Ir in NPs did not significantly affect the mean diameter or the zeta-potential values of the NPs. The unencapsulated drug was removed using a centrifugation method. In the literature, similar zeta potential value and particle size were reported.⁵⁷

Figure 3A shows the particle size distribution of NPs by dynamic light scattering which indicates monodispersed NP size

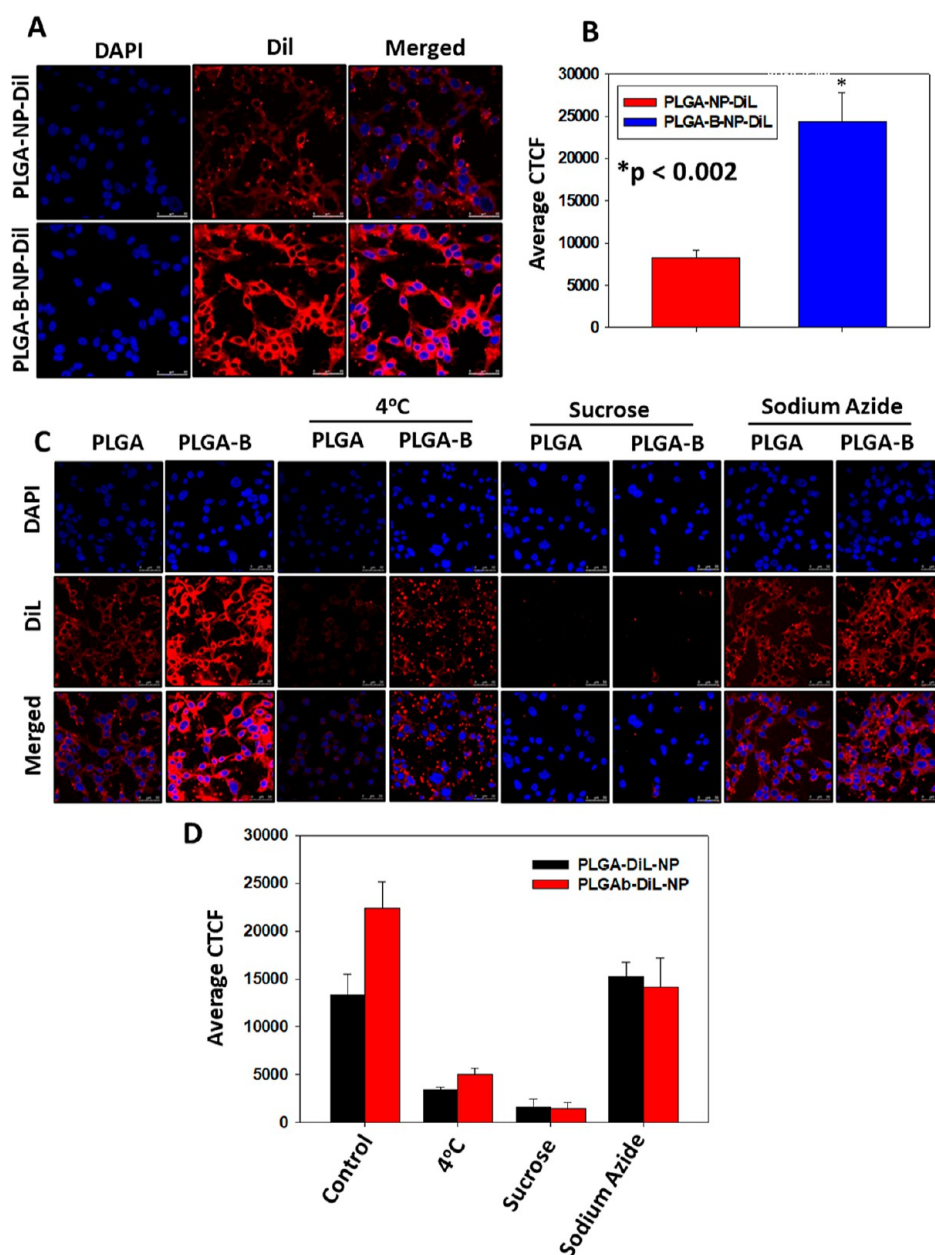


Figure 6. PLGA-B-NP-DiL NPs exhibit higher cellular uptake in colon cancer cells. (A) Intracellular uptake of PLGA-NP-DiL and PLGA-B-NP-DiL was monitored by confocal microscopy in CT-26 murine colon carcinoma cells. Briefly, cells grown on glass coverslips incubated with PLGA-NP-DiL and PLGA-B-NP-DiL for 4 h, mounted on glass slides, and images were captured. (B) Corrected total cell fluorescence (CTCF) of Cy5.5 was quantified from the images by NIH ImageJ software (ImageJ Freeware; <http://rsb.info.nih.gov/ij/>) and represented in the form of bar graph (mean \pm SEM). (C,D) Cells were treated with cold temp (4 °C), sucrose (0.5 M), and sodium azide (0.1%) for 1 h prior to treatment with NPs followed by confocal analysis. CTCF of Cy5.5 was quantified from the images by NIH ImageJ software (ImageJ Freeware; <http://rsb.info.nih.gov/ij/>) and represented in the form of bar graph (mean \pm SEM).

and their particles sizes are not significantly different. The inner structure of formulated NPs, was observed by TEM in order to confirm the structural characteristics. The size of the NPs was measured in a partially dried state. The average diameters were observed to be in the range of 15–25 nm. for PLGA-NP-Ir and PLGA-B-NP-Ir NPs, as shown in Figure 3B. Figure 3C depicts the images of NPs by AFM, which again confirmed the spherical morphology of NPs with uniform distribution.

Sizes and zeta potential of formulated NPs are in the similar range with the NPs reported in the literature using commercially available PLGA copolymers.⁵⁶

4.1. Wide Angle X-ray Diffraction of Powder Samples.

Figure 4A illustrates the diffraction pattern for Ir, PLGA, PLGA-B, Ir-loaded PLGA-NP-Ir, and PLGA-B-NP-Ir NPs. The WXR D spectra confirmed that Ir showed a sharp crystalline diffraction angle in the range $2\theta = 7-25^\circ$. PLGA and PLGA-B copolymer showed a decrease in the intensity, and broad diffraction peaks were observed which indicated the amorphous nature of the polymer. However, the diffraction peaks of the Ir did not appear, which confirmed its uniform distribution in PLGA-NP-Ir and PLGA-B-NP-Ir NPs.

4.2. Thermal Characterization by Differential Scanning Calorimetry Analysis.

The thermal behaviors of Ir,

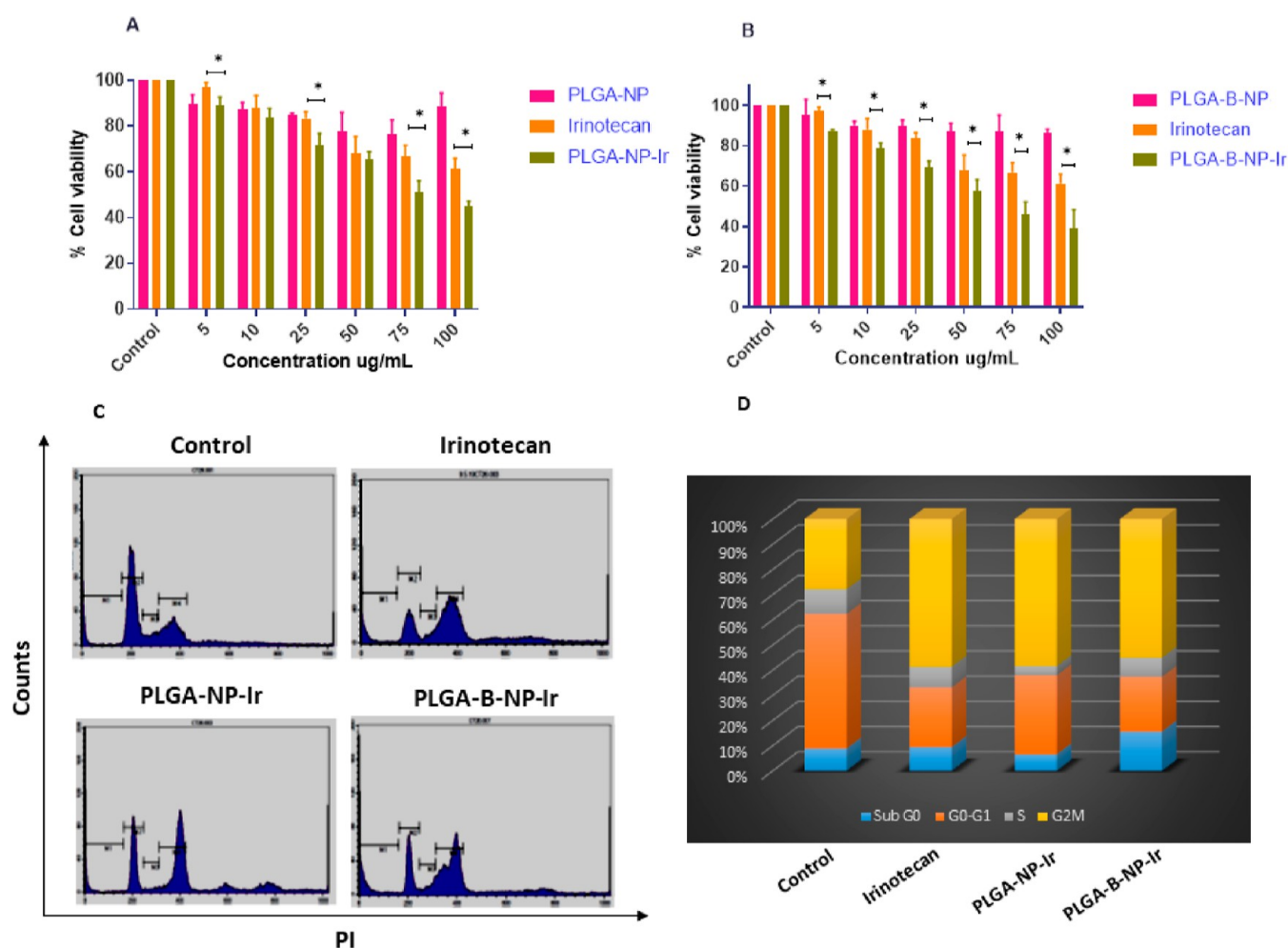


Figure 7. In vitro toxicity and cell cycle analysis: (A) CT-26 cells were treated either with blank PLGA-NP or with various Ir equivalent doses (0–100 $\mu\text{g}/\text{mL}$) of free Ir and PLGA-NP-Ir and cell viability was examined by the MTT assay. Error bars represent mean \pm SEM, $*p < 0.05$. (B) CT-26 cells were treated either with blank PLGA-B-NP or with various Ir equivalent doses (0–100 $\mu\text{g}/\text{mL}$) of free Ir and PLGA-B-NP-Ir and cell viability was examined by the MTT assay. Error bars represent mean \pm SEM, $*p < 0.05$. (C,D) Cell cycle analysis of CT-26 cells treated with Ir equivalent concentrations (50 $\mu\text{g}/\text{mL}$) of free Ir, and quantification for Ir-loaded NPs compared with free Ir, PLGA-NP-Ir, and PLGA-B-NP-Ir. Bar graph represents the percentage of cells in various cell cycle phases.

PLGA, PLGA-B, and Ir-loaded PLGA-NP-Ir and PLGA-B-NP-Ir were studied using DSC and are shown in Figure 4B. DSC curve showed the endothermic melting peak T_m at 245 $^{\circ}\text{C}$ demonstrating the crystalline nature of Ir. The T_g of the PLGA copolymer is at 30.8 $^{\circ}\text{C}$. PLGA-biotin displayed T_g at 41.8 $^{\circ}\text{C}$. PLGA-NP-Ir and PLGA-B-NP-Ir polymeric NPs showed the T_g at 15.4 and 21.2 $^{\circ}\text{C}$ respectively. The disappearance of the Ir melting point (T_m) in both PLGA-NP-Ir and PLGA-B-NP-Ir also confirmed the uniform distribution or amorphous phase transformation of Ir in the polymer matrix.^{49,58}

4.3. Release Profile In Vitro. The drug release profile and serum stability are shown in Figure 5A,B. It was observed that PLGA-NP-Ir and PLGA-B-NP-Ir exhibited a similar release profile (15–25% drug release) up to 1 h in the absence or presence of serum. In the absence of serum, a total of 40–50% of the drug was released over the first 24 h. In the presence of serum, approximately 60% of the drug was released over 24 h, where no significant release difference was observed. The NPs exhibited swelling in DMSO due to the solvent interaction. However, the in vitro release study of NPs was carried out in PBS and in 50% serum in PBS pH 7.4. The initial burst release of the irinotecan was possibly caused due to large surface area of the

NPs and the discharge of surface-bound irinotecan and the short diffusional distance.⁵⁹ The diffusion of irinotecan into the release medium [50% serum in PBS (pH 7.4)] is the key for better drug release and, in other words, the solubility of the drug in the medium.

In contrast, DMSO control showed the rapid release of the drug into the dialysate and more than 95% of the drug released within 24 h. Figure S14 shows the initial release study of NPs up to 24 h: (A) in PBS, pH 7.4, and (B) in 50% serum in PBS, pH 7.4. The sustained release of Ir up to 24 h from the polymeric matrix may be due to by diffusion/erosion. Figure S15A,B shows the percent drug released versus time (Korsic–Peppas model fitting with the equation). This model ascribes the mechanism of drug release from the polymeric NPs system, or when the release follows several kinetics mechanisms. The percent drug released versus time are fitted using this equation $M_t/M_{\infty} = K \cdot t^n$, where M_t/M_{∞} = percent drug released at time t , K = constant incorporating structural and geometrical characteristics of the sustained release device, and n = exponential which characterizes mechanism of drug release. If the dissolution time becomes somewhat longer, 100% irinotecan release cannot be obtained because the release of irinotecan molecules by diffusion will be

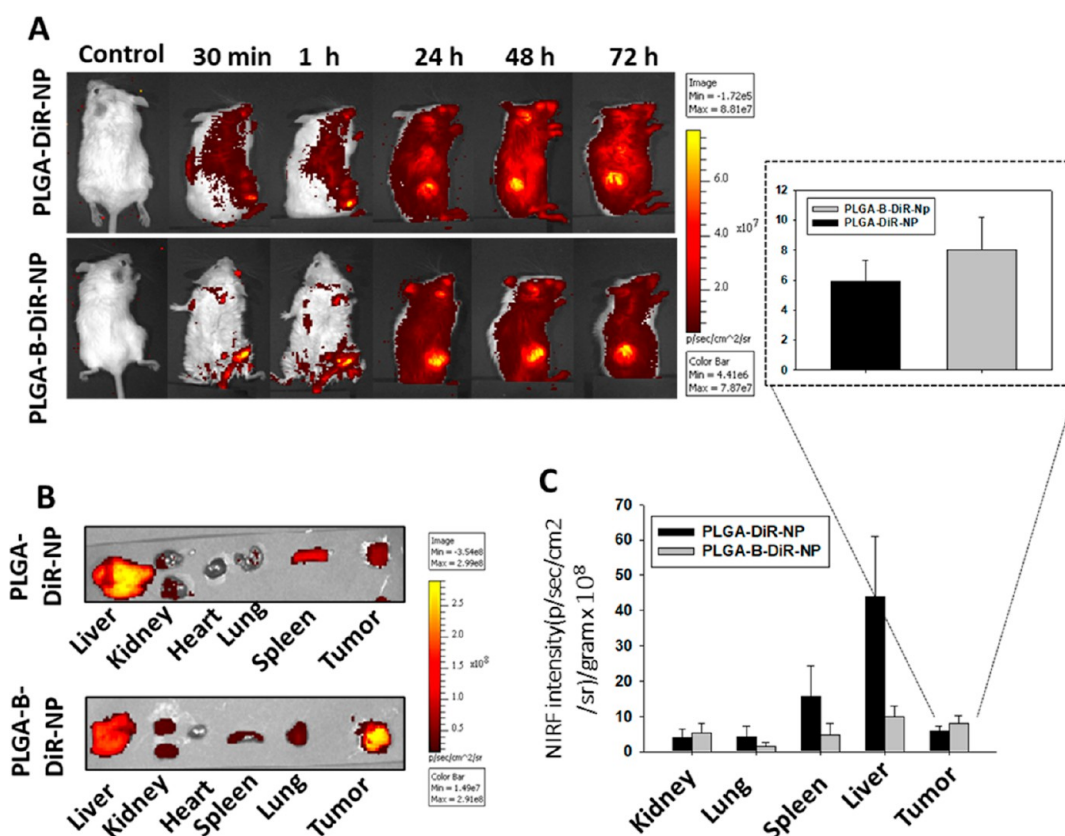


Figure 8. PLGA-B-NP-DiR NPs exhibit efficient active tumor targeting. (A) CT-26 tumor bearing BALB/c mice were treated with PLGA-NP-DiR and PLGA-B-NP-DiR intravenously, and NIRF images were taken at 30, 1, 24, 48, and 72 h ($n = 3$). (B) NIRF images of tumor and major organs dissected from PLGA-NP-DiR and PLGA-B-NP-DiR treated mice after 72 h, and the images were captured by ex vivo imaging at various time points. (C) NIRF intensity was measured using the region of interest and plotted in the form of bar graph (mean + SE, $n = 3$).

more difficult because of the physically cross-linked polymeric matrix formed because of several interactions. The similar release behavior has been observed for hydrophobic drugs.⁵⁹

4.4. In Vitro Cellular Uptake. Biotin-mediated targeting of NPs was established by an in vitro cellular uptake study in CT-26 cells using confocal laser scanning microscopy (CLSM). Dil dye was chosen because it does not react with the cell membrane and is a widely used carbocyanine membrane dye that labels cell membranes by inserting its two long (C_{18} carbon) hydrocarbon chains into the lipid bilayer. To confirm the intracellular delivery of the NPs loaded with DiI dye, CT-26 cells were treated with PLGA-NP-DiI and PLGA-B-NP-DiI NPs and fluorescence imaging and measurements were carried out by CLSM. The uptake of the NPs was confirmed by the presence of red signals, as revealed in Figure 6A. The results established the higher cellular uptake of PLGA-B-NP-DiI in CT-26 cells, as demonstrated by enhanced red fluorescence as compared to PLGA-NP-DiI. The quantitative estimation of the cellular uptake further supported these data (Figure 6B). Such results together with total fluorescence measurements showed the accomplishment of selective uptake and active targeting of biotin-targeted NPs in cancer cells overexpressing biotin receptors. To further examine the uptake mechanism of NPs, we treated CT-26 cells with PLGA-B-NP-DiI at 4 °C or with metabolic inhibitors such as hypertonic sucrose and sodium azide (NaN_3) at 37 °C. Figure 6C shows the reduced fluorescence which was observed in the CT-26 cells labeled with PLGA-B-NP-DiI NPs at 4 °C or pretreated with sucrose or NaN_3 . As lower temperature and metabolic inhibitors such as

sucrose and NaN_3 negatively affect the energy production in cells, lower uptake of NPs after pretreatment with these agents shows that the primary mechanism of cell uptake is an energy-dependent active endocytosis.

4.5. In Vitro Antitumor Efficacy Studies. The MTT assay was used to examine the in vitro antitumor activity of the Ir-loaded NPs in CT-26 murine colon carcinoma cells, as shown in Figure 7A,B. Cells were incubated with a range of drug concentrations (5–100 $\mu\text{g}/\text{mL}$) for 24 h. The data suggested that PLGA-NP-Ir and PLGA-B-NP-Ir showed improved cell toxicity against CT-26 cells as compared to free Ir. Competitive inhibition normally plays a certain important role on cells and living systems. In living organisms, the products of enzymatic reactions are involved in numerous cell signaling and regulatory pathways, together with those that initiate cellular activities, for instance, cell division and growth, which regulate the function of tissues and organ systems. The products from competitive inhibition can significantly alter cell and system function. Therefore, a competitive inhibition control might be a better way to confirm targeting. Here, biotin-conjugated PLGA-containing irinotecan NPs may bind with *p*-glycoprotein suppressing biotin molecules and blocks the production of nucleic acids that are necessary for DNA synthesis. Furthermore, the cell cycle analysis after treatment with Ir, PLGA-NP-Ir, and PLGA-B-NP-Ir is shown in Figure 7C,D. The results suggested that free drug (Ir), as well as Ir-loaded NPs, induced cell cycle arrest in the G2M phase of cell cycle which might be the cause for subsequent apoptosis. However, PLGA-B-NP-Ir induced higher cell death as depicted by the increase in sub G0

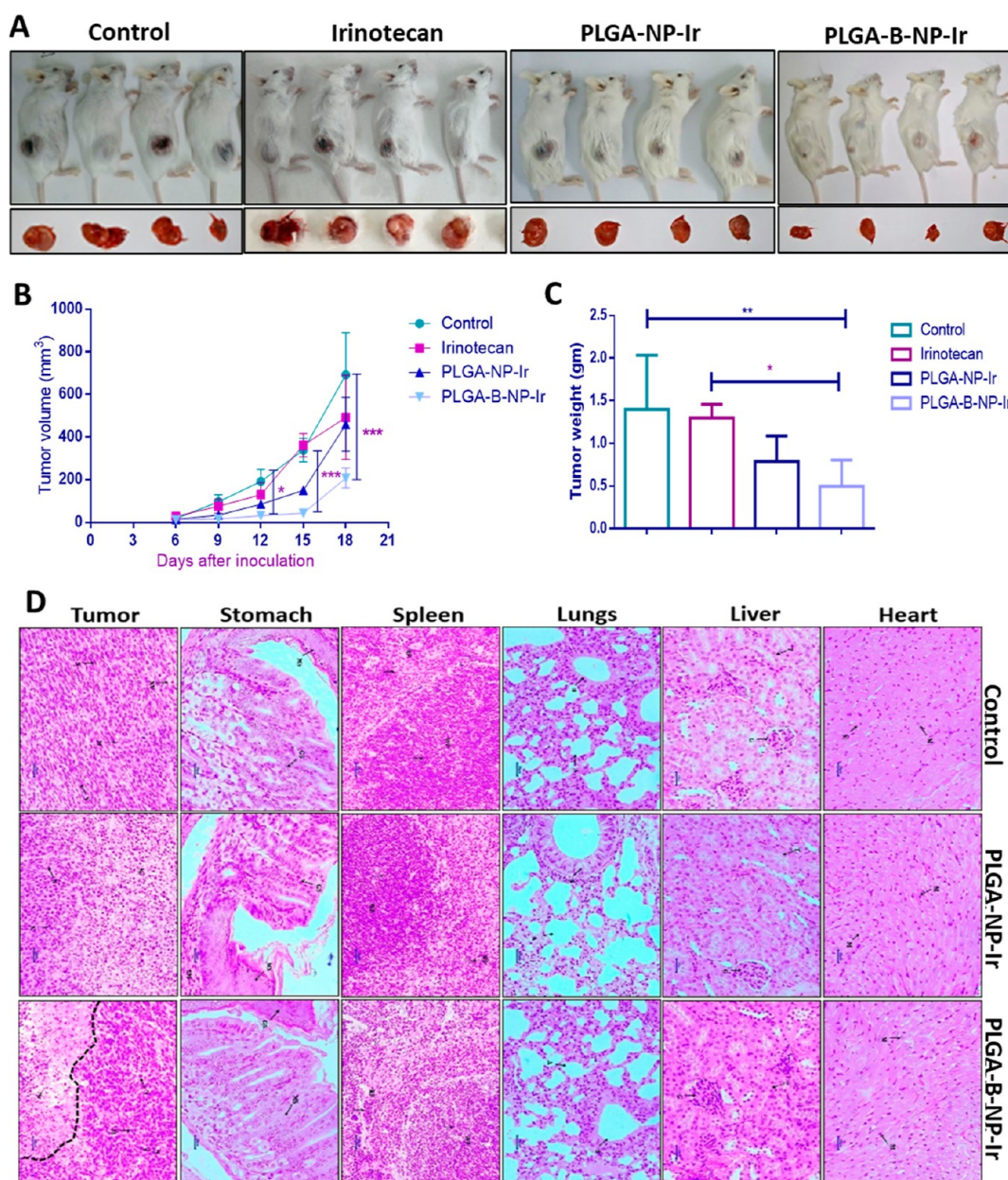


Figure 9. In vivo antitumor efficacy of nanoformulations: (A) Digital photographs of tumor bearing mice and excised tumors from different groups after sacrifice. (B) Tumor volumes were calculated and analyzed statistically. The graph represents the change in mean tumor volume with respect to time \pm SE, $n = 4$. (C) Tumors were excised, weighed, and analyzed statistically. Bar graph represents mean tumor weight \pm SD, $n = 4$. (D) H & E images of tumor slices after treatment with NPs. The scale bar is 20 μ m. * $p < 0.1$, ** $p < 0.01$, *** $p < 0.001$, and n.s. representing no significance.

population in PLGA-B-NP-Ir NPs-treated cells as compared to free Ir and PLGA-NP-Ir. Hence, PLGA-B-NP-Ir showed better antitumor efficacy with IC_{50} of 65 μ g/mL against free Ir (125 μ g/mL) due to the active targeting of the NPs which is statistically significant (p -value < 0.05) as compared to Ir as depicted in Figure 7A,B.⁴⁹

4.6. In Vivo Tumor Imaging. In vivo fluorescence imaging of PLGA-NP-DiR and PLGA-B-NP-DiR NPs was performed to identify the tumor targeting ability and biodistribution of the NPs in living mice bearing CT-26 biotin enriched colon tumor xenograft models. After systemic administration of DiR loaded NPs via tail vein, whole body imaging was monitored up to 72 h, as depicted in Figure 8A. The high intensity fluorescence was detected in tumor region in both PLGA-NP-DiR and PLGA-B-NP-DiR NPs treated mice which increases over time and

reached the maximum at 72 h, suggesting that these nanoformulations possess effective tumor targeting ability. Moreover, the higher fluorescence intensity was observed in PLGA-B-NP-DiR NP-treated mice as compared to PLGA-NP-DiR which can be attributed to selective active targeting which was achieved due to the PLGA surface decorated biotin ligand. In contrast to NP injected mice, no fluorescence signals were detected from control mice. The fluorescence image of excised organs is shown in Figure 8B where the highest fluorescence intensities were measured from the liver and spleen followed by tumors as compared to other organs. Fluorescence intensities from each organ were further computed, and the results are elaborated in Figure 8C. The rest of the tissues exhibit lower values which were anticipated from the fluorescence image. These in vivo and ex vivo imaging data proved that PLGA-B-NP-DiR NPs showed

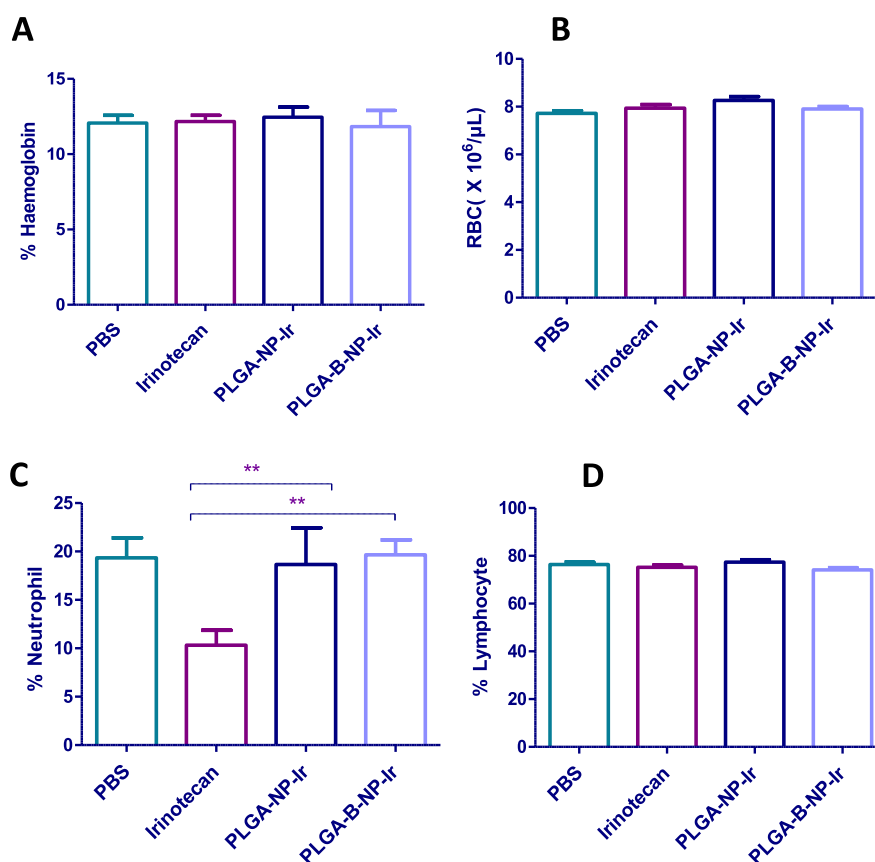


Figure 10. In vivo haematological parameter analysis (A) % haemoglobin, (B) RBC count (C) % neutrophil, and (D) % lymphocyte.

higher uptake in the tumor due to their selective uptake in biotin-enriched CT-26 cell bearing tumor and active targeting. Comparative study from fluorescence intensity graph as shown in Figure 8C, demonstrated that PLGA-B-NP-DiR have higher mean fluorescence intensity as compared to PLGA-NP-DiR suggesting higher uptake of these NPs. Interestingly, the lower accumulation of PLGA-B-NP-DiR was significantly observed in liver and spleen as compared to PLGA-NP-DiR, suggesting that active targeting via biotin reduced the nonspecific accumulation of NPs in normal tissue. Furthermore, in vivo tumor site retention of PLGA-NP-DiR and PLGA-B-NP-DiR in biotin-enriched colon tumor xenograft model up to 9 days, as shown in Figure S16A. PLGA-B-NP-DiR NPs showed better fluorescence intensity at the tumor site as compared to PLGA-NP-DiR NPs for longer duration as shown in Figure S16B. Overall, these findings indicate that PLGA-B-NP-DiR can actively target tumor tissue with higher retention while reducing nonspecific biodistribution which would lead to higher therapeutic efficacy with lower toxic side effects.

4.7. In Vivo Antitumor Efficacy Studies. The in vivo anticancer potential of Ir, PLGA-NP-Ir, and PLGA-B-NP-Ir NPs was studied in CT-26 in vivo tumor models. Mice were treated with four doses of Ir (10 mg/kg) or PLGA-NP-Ir or PLGA-B-NP-Ir (Ir equivalent content) intratumoral, twice a week post tumor inoculation. The PLGA-NP-Ir and PLGA-B-NP-Ir showed a statistically significant difference in the delay of tumor growth as compared to the Ir and vehicle control group ($p < 0.001$), as depicted in Figure 9A,B. The tumor volume graph shows that rapid growth was observed for the control and Ir group and there was no statistically significant difference between the control and Ir treatment group. Among all the

groups, the PLGA-B-NP-Ir-treated group exerts the strongest tumor growth inhibition. After the sacrifice, tumor weights for different treatment groups were measured and results are illustrated in Figure 9C. The data exhibited that PLGA-B-NP-Ir treated mice have significantly lower tumor weight as compared to the other groups, indicating superior antitumor efficacy of these NPs. Furthermore, to confirm the safety of the NPs, mice injected with different NPs, were sacrificed after completion of the treatment and the major organs such as liver, heart, lung, spleen, tumor, stomach, and kidney were collected and sliced for histology analysis with H & E images, as shown in Figure 9D. No noticeable tissue abnormality or n.s. or adverse effects was detected for each treatment group, which showed biocompatibility of all NPs. Therefore, the results suggested that Ir-loaded NPs exhibited no obvious toxicity in mice. Overall, these data depict that PLGA-B-NP-Ir treatment exerted the strongest tumor growth inhibition as evident from statistically significant results in the case of in vivo tumor delay in the Balb/C model without inducing any apparent toxicity in mice.

4.8. In Vivo Toxicity Study. Acute toxicity assessment of free Ir, PLGA-NP-Ir, and PLGA-B-NP-Ir groups was performed in healthy BALB/c mice after treatment with Ir equivalent doses (20 mg/kg). These NPs were administrated by oral route every day for 1 week. The blood routine examination and biochemical examination were tested after 1 week. Hematological parameters are depicted in Table S3 and Figure 10A–D and the results showed no significant effect on the treatment group except decrement percentage of neutrophil count for the Ir treatment group. The percentage of neutrophil count for the Ir treatment group was lower as compared to PLGA-NP-Ir and PLGA-B-NP-Ir NPs treatment group where the statistically significant

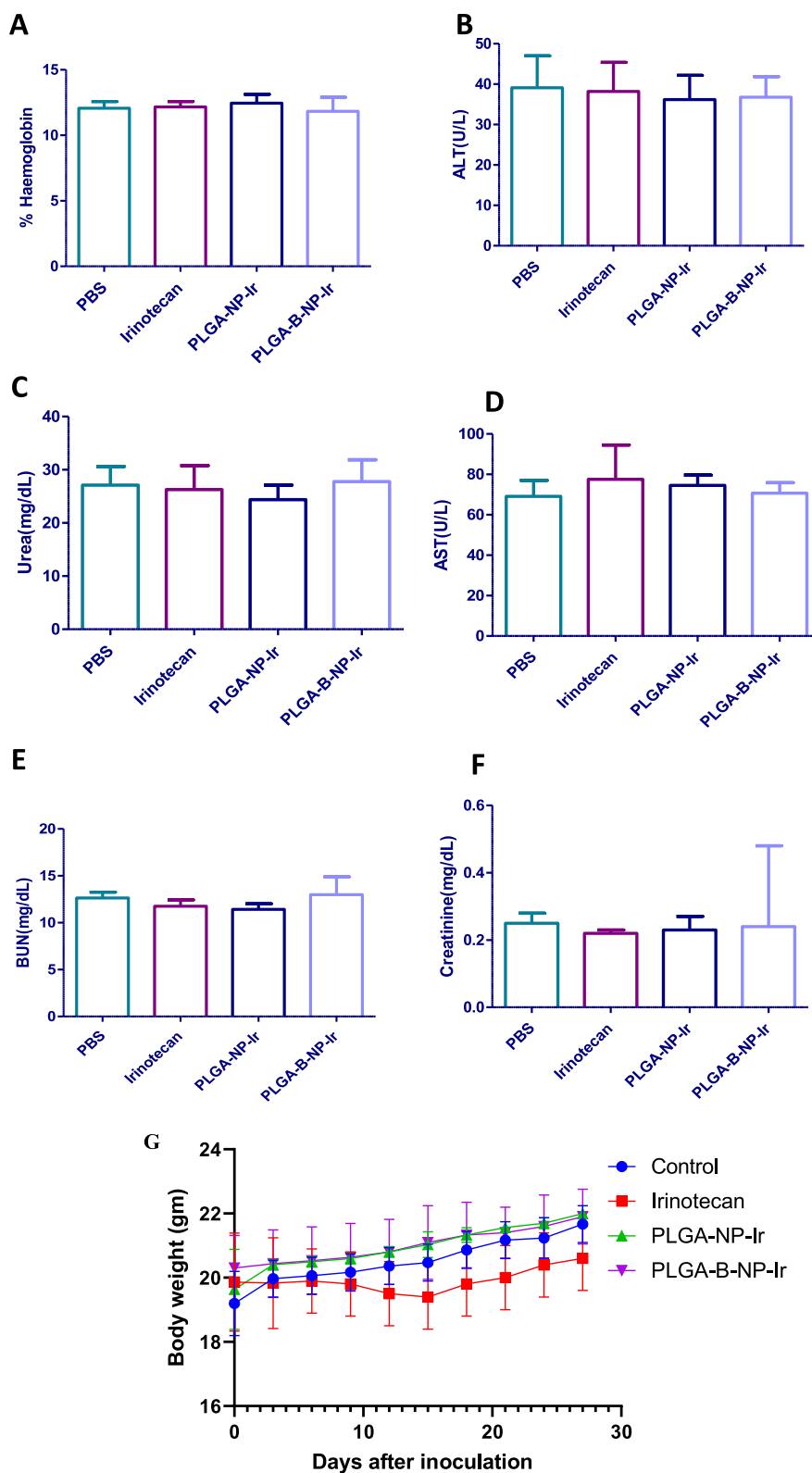


Figure 11. In vivo toxicity study for liver and kidney biomarker: (A) hemoglobin, (B) alanine transaminase (ALT), (C) urea, (D) aspartate transaminase (AST), (E) blood urea and nitrogen (BUN), (F) creatinine, and (G) body weight change.

difference ($P < 0.05$) was observed, as shown in Figure 10C. For other treatment groups of NPs, the result normally indicates that these NPs decrease the side effect of neutropenia associated with Ir. To examine the probable toxicity of NPs on the kidney and liver, biochemical analysis of kidney and liver function markers

was performed. Figure 11 shows the results of liver and kidney biomarkers, and the result demonstrated no significant change in the apparent toxicity. After 1 week of treatment, mice were sacrificed and histopathological evaluation was carried out with H & E staining with slices of major organs such as liver, heart,

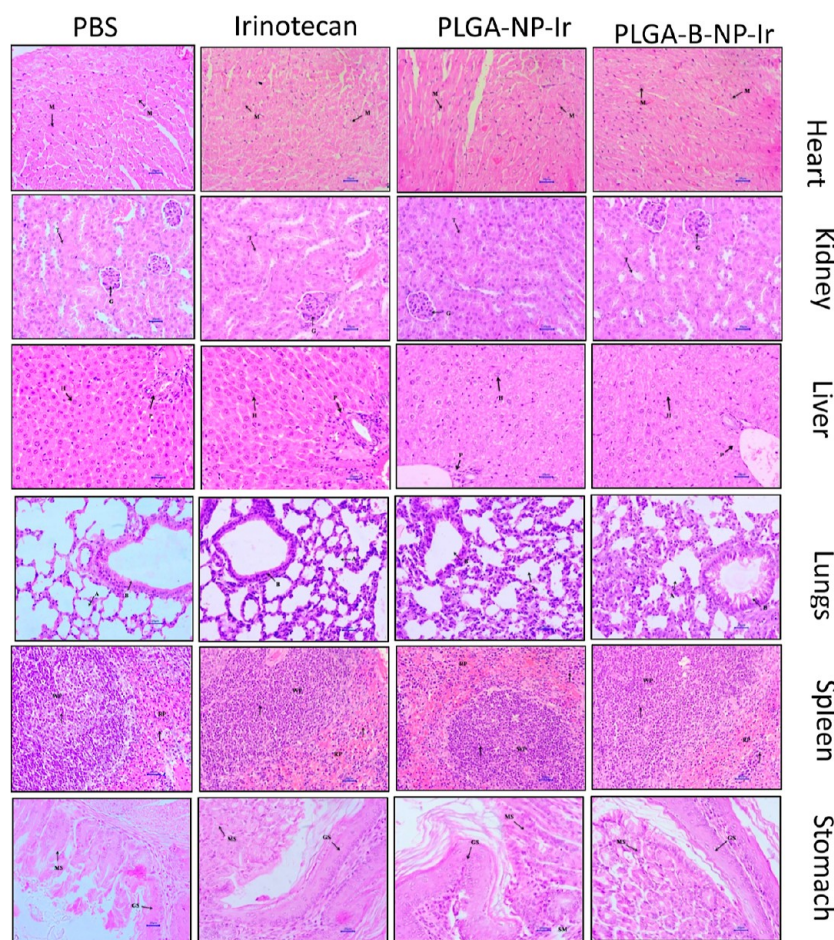


Figure 12. Histopathological study H & E images of mice organs after the treatment. The scale bar is 20 μm for safety study.

kidney, lungs, stomach, and spleen, as shown in Figure 12. The toxicity results showed that no significant difference was observed except for hematological analysis. The safety evaluation of NPs was studied successfully, and these NPs demonstrated biocompatibility as no abnormality and defect was observed. The body weight changes of mice monitored for all different groups under the study did not show $\leq 5\%$ changes which confirmed nontoxicity and safety of Ir loaded nano-carriers, as shown in Figure 11G.

Acute toxicity study confirmed safety and nontoxicity of these NPs in Balb/C mice at 20 mg/kg. In this study, Ir or Ir equivalent NPs of 20 mg/kg was given once a day for 1 week which was lowest dose as compared to literature dose of 30–60 mg/kg.⁶⁰ Neutropenia side effect of Ir was reported with PLGA-NP-Ir and PLGA-B-NP-Ir which was a serious dose limiting side effect of Ir. The drug (irinotecan) in tumor immunity is not fully explored until date. However, literature study reveals that the depletion of immunosuppressive regulatory T cells occurs due to irinotecan.⁵⁹ In this study, the irinotecan and its NP have not altered blood leukocyte populations, which was attributed to insufficient dose (irinotecan) to lessen the cells populations or the cell numbers during sampling period. Furthermore, we emphasize the achievement of the antitumor activity without the neutropenia associated with irinotecan. The result obtained from PLGA-B-NP-Ir NPs is highly promising and demonstrated as an effective nanomedicine in the field of active targeted drug delivery. The PLGA-B-Ir nanoformulation might be an alternative for commercially available Onivyde, which is the

only FDA approved irinotecan nanoformulation made of PEGylated liposomes. This finding would be interesting in the future, especially when dual chemotherapy drugs will be used.

5. CONCLUSIONS

The PLGA copolymer was synthesized from D,L-lactide and glycolide in the presence of zinc proline complex using the ring opening polymerization technique which was confirmed as a biocompatible and safe initiator. The molecular weight and PDI of PLGA were confirmed by GPC. The range of weight-average molecular weight (\bar{M}_w) was observed in the range of 11,000 to 90,000 Da. However, PLGA copolymer ($\bar{M}_w = 21000$ Da) and biotin-conjugated PLGA were used for further formulation study. The MALDI-TOF analysis of the PLGA copolymer showed the presence of end groups such as carboxyl and hydroxyl groups. DSC and XRD studies confirmed its amorphous nature. The chemical structure of biotin-conjugated PLGA was confirmed by ^1H NMR and HABA–avidin colorimetric assay. The polymeric formulations were prepared by the nanoprecipitation method using Cremophor RH 40 as the surfactant. The encapsulation efficiency of Ir was achieved $\sim 88\%$ and exhibited sustained drug release profiles in the absence, or presence of 50% serum. Effective cell killing was achieved in CT-26 cells in vitro which was higher for PLGA-B-NP-Ir as compared to PLGA-NP-Ir. The prolonged blood circulation profile and good tumor accumulation were observed in the presence of PLGA-B-NP-Ir which facilitated the active targeting in addition to the EPR effect, resulting in a delay in

significant tumor growth after multiple systemic injections in mice model as compared with PLGA-NP-Ir. The overall promising results suggest the potential application of the synthesized biotin-conjugated PLGA polymer as a matrix for Ir NP (PLGA-B-NP-Ir) in an active targeted drug delivery application for colon cancer.

■ ASSOCIATED CONTENT

SI Supporting Information

The Supporting Information is available free of charge at <https://pubs.acs.org/doi/10.1021/acsomega.3c07833>.

Selected NMR spectrum including ^{13}C NMR spectrum of PLGA, size exclusion chromatography of synthesized PLGA (PLGA-1 to PLGA-10), MALDI-TOF spectrum of PLGA by using the DHB matrix, colorimetric analysis of biotin on surface decorated PLGA by the avidine–HABA colorimetric assay, in vitro release study of nanoparticles in PBS and in 50% serum in PBS (initial 24 h release profile) and release kinetics model, Korsmeyer–Peppas model fitting with the equation, tumor site retention study, in vivo tumor site retention study, NIRF intensity for tumor site retention study, results of formulation optimization of nanoparticle formulation, physicochemical properties for optimization of nanoparticle, and hematological analysis (PDF)

■ AUTHOR INFORMATION

Corresponding Author

Baijyantimala Garnaik – Polymer Science and Engineering Division, CSIR-National Chemical Laboratory, Pune 411008, India; Academy of Scientific and Innovative Research AcSIR Headquarters, Ghaziabad, Uttar Pradesh 201 002, India; orcid.org/0000-0003-4264-0316; Phone: +91-20-25902071; Email: garnaikncl@gmail.com; Fax: +91-20-25902615

Authors

Prabhanjan S. Giram – Polymer Science and Engineering Division, CSIR-National Chemical Laboratory, Pune 411008, India; Academy of Scientific and Innovative Research AcSIR Headquarters, Ghaziabad, Uttar Pradesh 201 002, India; orcid.org/0000-0003-0439-1347

Ramakrishna Nimma – Laboratory of Tumor, Biology, Angiogenesis and Nanomedicine Research, National Center for Cell Science, Pune 411007, India

Anuradha Bulbule – Laboratory of Tumor, Biology, Angiogenesis and Nanomedicine Research, National Center for Cell Science, Pune 411007, India

Amit Singh Yadav – Laboratory of Tumor, Biology, Angiogenesis and Nanomedicine Research, National Center for Cell Science, Pune 411007, India; orcid.org/0000-0002-5118-4538

Mahadeo Gorain – Laboratory of Tumor, Biology, Angiogenesis and Nanomedicine Research, National Center for Cell Science, Pune 411007, India

Nalukurthi Naga Venkata Radharani – Laboratory of Tumor, Biology, Angiogenesis and Nanomedicine Research, National Center for Cell Science, Pune 411007, India

Gopal C. Kundu – School of Biotechnology and Kalinga Institute of Medical Sciences (KIMS), KIIT Deemed to be University, Institute of Eminence, Bhubaneswar 751 024, India

Complete contact information is available at:

<https://pubs.acs.org/10.1021/acsomega.3c07833>

Notes

The authors declare no competing financial interest.

■ ACKNOWLEDGMENTS

P.S.G. acknowledges the University Grant Commission, India for his doctoral research fellowship. This work was financially supported by the Council of Scientific and Industrial Research, Government of India, New Delhi (CSC-0302 and CSC-0134).

■ REFERENCES

- (1) Vert, M.; Schwach, G.; Coudane, J. Present and Future of PLA Polymers. *J. Macromol. Sci., Part A: Pure Appl. Chem.* **1995**, *32* (4), 787–796.
- (2) Jürgens, C.; Porte, T.; Wolter, D.; Schmidt, H. G.; Kricheldorf, H. R.; Kreiser-Saunders, I. [Development and characterization of an absorbable temporary wound dressing]. *Unfallchirurg* **1995**, *98* (4), 233–240.
- (3) Rasal, R. M.; Janorkar, A. V.; Hirt, D. E. “Poly (lactic acid) modifications”. *Prog. Polym. Sci.* **2010**, *35* (3), 338–356.
- (4) Doppalapudi, S.; Jain, A.; Khan, W.; Domb, A. J. Biodegradable Polymers—an Overview. *Polym. Adv. Technol.* **2014**, *25* (5), 427–435.
- (5) Doppalapudi, S.; Katiyar, S.; Domb, A. J.; Khan, W. Biodegradable Natural Polymers. In *Advanced Polymers in Medicine*; Puoci, F., Ed.; Springer International Publishing: Cham, 2015; pp 33–66.
- (6) Dunn, R. The Atrigel Drug Delivery System. *Modified-Release Drug Delivery Technology*; CRC Press, 2002.
- (7) Benicewicz, B. C.; Hopper, P. K. Review: Polymers for Absorbable Surgical Sutures—Part I. *J. Bioact. Compat. Polym.* **1990**, *5* (4), 453–472.
- (8) Benicewicz, B. C.; Hopper, P. K. Review: Polymers for Absorbable Surgical Sutures—Part II. *J. Bioact. Compat. Polym.* **1991**, *6* (1), 64–94.
- (9) Jain, A.; Kunduru, K. R.; Basu, A.; Mizrahi, B.; Domb, A. J.; Khan, W. Injectable Formulations of Poly(Lactic Acid) and Its Copolymers in Clinical Use. *Adv. Drug Delivery Rev.* **2016**, *107*, 213–227.
- (10) Wischke, C.; Schwendeman, S. P. Principles of encapsulating hydrophobic drugs in PLA/PLGA microparticles. *Int. J. Pharm.* **2008**, *364* (2), 298–327.
- (11) Wright, J. C.; Hoffman, A. S. Historical Overview of Long Acting Injections and Implants. In *Long Acting Injections and Implants*; Wright, J. C., Burgess, D. J., Eds.; *Advances in Delivery Science and Technology*; Springer US: Boston, MA, 2012; pp 11–24.
- (12) Uhrich, K. E.; Cannizzaro, S. M.; Langer, R. S.; Shakesheff, K. M. Polymeric Systems for Controlled Drug Release. *Chem. Rev.* **1999**, *99* (11), 3181–3198.
- (13) Zivkovic, L.; Akar, B.; Roux, B. M.; Spremo Potparevic, B.; Bajic, V.; Brey, E. M. Investigation of DNA Damage in Cells Exposed to Poly (Lactic-Co-Glycolic Acid) Microspheres. *J. Biomed. Mater. Res., Part A* **2017**, *105* (1), 284–291.
- (14) Yu, L.; Zhang, Z.; Ding, J. Influence of LA and GA Sequence in the PLGA Block on the Properties of Thermogelling PLGA-PEG-PLGA Block Copolymers. *Biomacromolecules* **2011**, *12* (4), 1290–1297.
- (15) Microstructural analysis of poly[(l,l-lactide)-co-(glycolide)] by ^1H and ^{13}C n.m.r. spectroscopy—ScienceDirect. <https://www.sciencedirect.com/science/article/abs/pii/S03043886196810883> (accessed June 05, 2022).
- (16) Giram, P. S.; Garnaik, B. Evaluation of Biocompatibility of Synthesized Low Molecular Weight PLGA Copolymers Using Zinc L-Proline through Green Route for Biomedical Application. *Polym. Adv. Technol.* **2021**, *32* (11), 4502–4515.
- (17) Giram, P. S.; Wang, J. T. W.; Walters, A. A.; Rade, P. P.; Akhtar, M.; Han, S.; Faruqi, F. N.; Abdel-Bar, H. M.; Garnaik, B.; Al-Jamal, K. T. Green Synthesis of Methoxy-Poly(Ethylene Glycol)-Block-Poly(l-Lactide-Co-Glycolide) Copolymer Using Zinc Proline as a Biocompatible Initiator for Irinotecan Delivery to Colon Cancer in Vivo. *Biomater. Sci.* **2021**, *9* (3), 795–806.

- (18) Jeevarathinam, A. S.; Lemaster, J. E.; Chen, F.; Zhao, E.; Jokerst, J. V. Photoacoustic Imaging Quantifies Drug Release from Nanocarriers via Redox Chemistry of Dye-Labeled Cargo. *Angew. Chem., Int. Ed.* **2020**, *59* (12), 4678–4683.
- (19) Wu, C. Systemic Therapy for Colon Cancer. *Surg. Oncol. Clin.* **2018**, *27* (2), 235–242.
- (20) Escoffre, J.-M.; Novell, A.; Serrière, S.; Lecomte, T.; Bouakaz, A. Irinotecan Delivery by Microbubble-Assisted Ultrasound: In Vitro Validation and a Pilot Preclinical Study. *Mol. Pharmaceutics* **2013**, *10* (7), 2667–2675.
- (21) Sequential versus combination chemotherapy with capecitabine, irinotecan, and oxaliplatin in advanced colorectal cancer (CAIRO): a phase III randomised controlled trial—ScienceDirect. <https://www.sciencedirect.com/science/article/abs/pii/S0140673607610861> (accessed June 05, 2022).
- (22) Cremonini, C.; Loupakis, F.; Antoniotti, C.; Lupi, C.; Sensi, E.; Lonardi, S.; Mezi, S.; Tomasello, G.; Ronzoni, M.; Zaniboni, A.; Tonini, G.; Carlomagno, C.; Allegrini, G.; Chiara, S.; D'Amico, M.; Granetto, C.; Cazzaniga, M.; Boni, L.; Fontanini, G.; Falcone, A. FOLFOXIRI plus Bevacizumab versus FOLFIRI plus Bevacizumab as First-Line Treatment of Patients with Metastatic Colorectal Cancer: Updated Overall Survival and Molecular Subgroup Analyses of the Open-Label, Phase 3 TRIBE Study. *Lancet Oncol.* **2015**, *16* (13), 1306–1315.
- (23) Bae, Y. H.; Park, K. Advanced drug delivery 2020 and beyond: Perspectives on the future. *Adv. Drug Delivery Rev.* **2020**, *158*, 4–16.
- (24) Wicki, A.; Witzigmann, D.; Balasubramanian, V.; Huwyler, J. Nanomedicine in Cancer Therapy: Challenges, Opportunities, and Clinical Applications. *J. Controlled Release* **2015**, *200*, 138–157.
- (25) Gu, F. X.; Karnik, R.; Wang, A. Z.; Alexis, F.; Levy-Nissenbaum, E.; Hong, S.; Langer, R. S.; Farokhzad, O. C. Targeted Nanoparticles for Cancer Therapy. *Nano Today* **2007**, *2* (3), 14–21.
- (26) Zhong, Y.; Meng, F.; Deng, C.; Zhong, Z. Ligand-Directed Active Tumor-Targeting Polymeric Nanoparticles for Cancer Chemotherapy. *Biomacromolecules* **2014**, *15* (6), 1955–1969.
- (27) Nanoparticle-based oral delivery systems for colon targeting: principles and design strategies—ScienceDirect. <https://www.sciencedirect.com/science/article/abs/pii/S2095927316301281> (accessed June 05, 2022).
- (28) El-Hammadi, M. M.; Delgado, Á. V.; Melguizo, C.; Prados, J. C.; Arias, J. L. Folic Acid-Decorated and PEGylated PLGA Nanoparticles for Improving the Antitumor Activity of 5-Fluorouracil. *Int. J. Pharm.* **2017**, *516* (1–2), 61–70.
- (29) Ren, W. X.; Han, J.; Uhm, S.; Jang, Y. J.; Kang, C.; Kim, J.-H.; Kim, J. S. Recent Development of Biotin Conjugation in Biological Imaging, Sensing, and Target Delivery. *Chem. Commun.* **2015**, *51* (52), 10403–10418.
- (30) Gao, Q.; Lan, P.; Shao, H.; Hu, X. Direct Synthesis with Melt Polycondensation and Microstructure Analysis of Poly(L-Lactic Acid-Co-Glycolic Acid). *Polym. J.* **2002**, *34* (11), 786–793.
- (31) Maiti, S.; Paira, P. Biotin Conjugated Organic Molecules and Proteins for Cancer Therapy: A Review. *Eur. J. Med. Chem.* **2018**, *145*, 206–223.
- (32) Grafe, F.; Brandsch, M.; Wohlrab, W.; Neubert, R. H. Transport of Biotin in Human Keratinocytes. *J. Invest. Dermatol.* **2003**, *120* (3), 428–433.
- (33) Mehdizadeh, M.; Rouhani, H.; Sepehri, N.; Varshochian, R.; Ghahremani, M. H.; Amini, M.; Gharghabi, M.; Ostad, S. N.; Atyabi, F.; Baharian, A.; Dinarvand, R. Biotin Decorated PLGA Nanoparticles Containing SN-38 Designed for Cancer Therapy. *Artif. Cells, Nanomed., Biotechnol.* **2017**, *45* (3), 495–504.
- (34) Rompicharla, S. V. K.; Kumari, P.; Bhatt, H.; Ghosh, B.; Biswas, S. Biotin Functionalized PEGylated Poly(Amidoamine) Dendrimer Conjugate for Active Targeting of Paclitaxel in Cancer. *Int. J. Pharm.* **2019**, *557*, 329–341.
- (35) Biotin decorated sunitinib loaded nanostructured lipid carriers for tumor targeted chemotherapy of lung cancer—ScienceDirect. <https://www.sciencedirect.com/science/article/abs/pii/S1773224718312577> (accessed June 05, 2022).
- (36) Dai, Y.; Xing, H.; Song, F.; Yang, Y.; Qiu, Z.; Lu, X.; Liu, Q.; Ren, S.; Chen, X.; Li, N. Biotin-Conjugated Multilayer Poly [D,L-Lactide-Co-Glycolide]-Lecithin-Polyethylene Glycol Nanoparticles for Targeted Delivery of Doxorubicin. *J. Pharm. Sci.* **2016**, *105* (9), 2949–2958.
- (37) Fahrer, J.; Schweitzer, B.; Fiedler, K.; Langer, T.; Gierschik, P.; Barth, H. C2-Streptavidin Mediates the Delivery of Biotin-Conjugated Tumor Suppressor Protein P53 into Tumor Cells. *Bioconjugate Chem.* **2013**, *24* (4), 595–603.
- (38) Pramanik, A. K.; Siddikuzzaman; Palanimuthu, D.; Somasundaram, K.; Samuelson, A. G. Biotin Decorated Gold Nanoparticles for Targeted Delivery of a Smart-Linked Anticancer Active Copper Complex: In Vitro and In Vivo Studies. *Bioconjugate Chem.* **2016**, *27* (12), 2874–2885.
- (39) Parwe, S. P.; Warkad, S. D.; Mane, M. V.; Shedage, P. S.; Garnaik, B. Investigation of the biocompatibility and cytotoxicity associated with ROP initiator and its role in bulk polymerization of l-lactide. *Polymer* **2017**, *111*, 244–251.
- (40) Shyamroy, S.; Garnaik, B.; Sivaram, S. High Molecular Weight Poly(L-Lactic Acid)s by Polyesterification Using Diisopropylcarbodiimide (DIPC) and 4-(Dimethylamino) Pyridinium-p-Toluene Sulfonate (DPTS). *Polym. Bull.* **2015**, *72* (3), 405–415.
- (41) Final report of the safety assessment of Urea. *Int. J. Toxicol.* **2005**, *24*(3), 1–56.
- (42) El-Gogary, R. I.; Gaber, S. A. A.; Nasr, M. Polymeric Nanocapsular Baicalin: Chemometric Optimization, Physicochemical Characterization and Mechanistic Anticancer Approaches on Breast Cancer Cell Lines. *Sci. Rep.* **2019**, *9* (1), 11064.
- (43) Zhu, Q.; Bao, B.; Zhang, Q.; Yu, J.; Lu, W. Maleimidation of Dextran and the Application in Designing a Dextran-Camptothecin Conjugate. *RSC Adv.* **2018**, *8* (5), 2818–2823.
- (44) Illes, B.; Wuttke, S.; Engelke, H. Liposome-Coated Iron Fumarate Metal-Organic Framework Nanoparticles for Combination Therapy. *Nanomaterials (Basel)* **2017**, *7* (11), No. E351.
- (45) Honrubia-Gómez, P.; López-Garrido, M. P.; Gil-Gas, C.; Sánchez-Sánchez, J.; Alvarez-Simon, C.; Cuenca-Escalona, J.; Perez, A. F.; Arias, E.; Moreno, R.; Sánchez-Sánchez, F.; Ramirez-Castillejo, C. Pdf Derived Peptides Affect Colorectal Cancer Cell Lines Resistance and Tumour Re-Growth Capacity. *Oncotarget* **2019**, *10* (31), 2973–2986.
- (46) Zare, E. N.; Jamaledin, R.; Naserzadeh, P.; Afjeh-Dana, E.; Ashtari, B.; Hosseinzadeh, M.; Vecchione, R.; Wu, A.; Tay, F. R.; Borzacchiello, A.; Makvandi, P. Metal-Based Nanostructures/PLGA Nanocomposites: Antimicrobial Activity, Cytotoxicity, and Their Biomedical Applications. *ACS Appl. Mater. Interfaces* **2020**, *12* (3), 3279–3300.
- (47) Park, K.; Skidmore, S.; Hadar, J.; Garner, J.; Park, H.; Otte, A.; Soh, B. K.; Yoon, G.; Yu, D.; Yun, Y.; Lee, B. K.; Jiang, X.; Wang, Y. Injectable, Long-Acting PLGA Formulations: Analyzing PLGA and Understanding Microparticle Formation. *J. Controlled Release* **2019**, *304*, 125–134.
- (48) Yu, L.; Zhang, Z.; Zhang, H.; Ding, J. Biodegradability and Biocompatibility of Thermoreversible Hydrogels Formed from Mixing a Sol and a Precipitate of Block Copolymers in Water. *Biomacromolecules* **2010**, *11* (8), 2169–2178.
- (49) Pereira, E. D.; Cerruti, R.; Fernandes, E.; Peña, L.; Saez, V.; Pinto, J. C.; Ramón, J. A.; Oliveira, G. E.; Souza Júnior, F. G. d. Influence of PLGA and PLGA-PEG on the Dissolution Profile of Oxaliplatin. *Polímeros* **2016**, *26*, 137–143.
- (50) Cheng, M.; Zhu, W.; Li, Q.; Dai, D.; Hou, Y. Anti-Cancer Efficacy of Biotinylated Chitosan Nanoparticles in Liver Cancer. *Oncotarget* **2017**, *8* (35), 59068–59085.
- (51) Singh, Y.; Durga Rao Viswanadham, K. K.; Kumar Jajoriya, A.; Meher, J. G.; Raval, K.; Jaiswal, S.; Dewangan, J.; Bora, H. K.; Rath, S. K.; Lal, J.; Mishra, D. P.; Chourasia, M. K. Click Biotinylation of PLGA Template for Biotin Receptor Oriented Delivery of Doxorubicin Hydrochloride in 4T1 Cell-Induced Breast Cancer. *Mol. Pharmaceutics* **2017**, *14* (8), 2749–2765.

(52) Mathijssen, R. H.; van Alphen, R. J.; Verweij, J.; Loos, W. J.; Nooter, K.; Stoter, G.; Sparreboom, A. Clinical Pharmacokinetics and Metabolism of Irinotecan (CPT-11). *Clin. Cancer Res.* **2001**, *7* (8), 2182–2194.

(53) Zhang, B.; Song, Y.; Wang, T.; Yang, S.; Zhang, J.; Liu, Y.; Zhang, N.; Garg, S. Efficient Co-Delivery of Immiscible Hydrophilic/Hydrophobic Chemotherapeutics by Lipid Emulsions for Improved Treatment of Cancer. *Int. J. Nanomed.* **2017**, *12*, 2871–2886.

(54) Ci, T.; Chen, L.; Yu, L.; Ding, J. Tumor Regression Achieved by Encapsulating a Moderately Soluble Drug into a Polymeric Thermogel. *Sci. Rep.* **2014**, *4* (1), 5473.

(55) Hill, M.; Cunningham, R. N.; Hathout, R. M.; Johnston, C.; Hardy, J. G.; Migaud, M. E. Formulation of Antimicrobial Tobramycin Loaded PLGA Nanoparticles via Complexation with AOT. *J. Funct. Biomater.* **2019**, *10* (2), 26.

(56) Yang, X.; Yang, Y.; Jia, Q.; Hao, Y.; Liu, J.; Huang, G. Preparation and Evaluation of Irinotecan Poly(Lactic-Co-Glycolic Acid) Nanoparticles for Enhanced Anti-Tumor Therapy. *AAPS PharmSciTech* **2019**, *20* (3), 133.

(57) Klippstein, R.; Wang, J. T.-W.; El-Gogary, R. I.; Bai, J.; Mustafa, F.; Rubio, N.; Bansal, S.; Al-Jamal, W. T.; Al-Jamal, K. T. Passively Targeted Curcumin-Loaded PEGylated PLGA Nanocapsules for Colon Cancer Therapy In Vivo. *Small* **2015**, *11* (36), 4704–4722.

(58) Liu, X.; Situ, A.; Kang, Y.; Villabroza, K. R.; Liao, Y.; Chang, C. H.; Donahue, T.; Nel, A. E.; Meng, H. Irinotecan Delivery by Lipid-Coated Mesoporous Silica Nanoparticles Shows Improved Efficacy and Safety over Liposomes for Pancreatic Cancer. *ACS Nano* **2016**, *10* (2), 2702–2715.

(59) Pulkkinen, M.; Pikkarainen, J.; Wirth, T.; Tarvainen, T.; Haapaaho, V.; Korhonen, H.; Seppala, J.; Jarvinen, K. Three-step tumor targeting of paclitaxel using biotinylated PLA-PEG nanoparticles and avidin–biotin technology: Formulation development and in vitro anticancer activity. *Eur. J. Pharm. Biopharm.* **2008**, *70* (1), 66–74.

(60) Fernandes, C.; Wanderley, C. W. S.; Silva, C. M. S.; Muniz, H. A.; Teixeira, M. A.; Souza, N. R. P.; Cândido, A. G. F.; Falcão, R. B.; Souza, M. H. L. P.; Almeida, P. R. C.; Câmara, L. M. C.; Lima-Júnior, R. C. P. Role of regulatory T cells in irinotecan-induced intestinal mucositis. *Eur. J. Pharm. Sci.* **2018**, *115*, 158–166.